Reconstructing past variations in environmental conditions and paleoproductivity over the last ~8000 years off north-central Chile (30° S)

Práxedes Muñoz[1,2], Lorena Rebolledo[3,4], Laurent Dezileau[5], Antonio Maldonado[2,6], Christoph Mayr[7,8], Paola Cárdenas[5,9], Carina B. Lange[4,10,11], Katherine Lalangui[10], Gloria Sanchez[12], Marco Salamanca[10], Karen Araya[1,13], Ignacio Jara[2], Gabriel Vargas[14], Marcel Ramos[1,2].

[1]Departamento de Biología Marina, Universidad Católica del Norte, Larrondo 1281, Coquimbo, Chile.
[2]Centro de Estudios Avanzados en Zonas Áridas (CEAZA), Coquimbo-La Serena, Chile.
[3]Departamento Científico, Instituto Antártico Chileno, Punta Arenas, Chile
[4]Centro FONDAP de Investigación Dinámica de Ecosistemas Marinos de Altas Latitudes (IDEAL), Universidad Austral de Chile, Campus Isla Teja, Valdivia, Chile.
[5]Normandie University, UNICAEN, UNIROUEN, CNRS, M2C, 14000 Caen, France.
[6]Instituto de Investigación Multidisciplinario en Ciencia y Tecnología, Universidad de La Serena, La Serena, Chile.
[7]Institut für Geographie, FAU Erlangen-Nürnberg, 91058 Erlangen, Germany.
[8]Department of Earth and Environmental Sciences & GeoBio-Center, LMU Munich, 80333 Munich.
[9]Programa Magister en Oceanografía, Universidad de Concepción, casilla 160C, Concepción, Chile.
[10]Departamento de Oceanografía, Facultad de Ciencias Naturales y Oceanográficas, Universidad de Concepción, Casilla 160C, Concepción, Chile.
[11]Centro de Investigación Oceanográfica COPAS Sur-Austral, Universidad de Concepción, Casilla 160C, Concepción, Chile.
[12]Universidad de Magallanes, Punta Arenas, Chile.
[13]Laboratoire Géosciences Montpellier (GM), Université de Montpellier, 34095 Montpellier Cedex 05, France.
[14]Departamento de Geología, Universidad de Chile, Santiago, Chile.

Correspondence to: Práxedes Muñoz (praxedes@ucn.cl)

Abstract

The Coquimbo (30°S) Region –located in the north-Central Chilean Coast– is characterized by relative dry summers and a short rainfall period during winter months. The wet-winter climate results from the interactions between the Southern Westerly Winds and the South Pacific Subtropical Anticyclone (SPSA). Inter-annual climate trends are mostly associated with El Niño-Southern Oscillation (ENSO), which produces high variability in precipitation. With the aim of establishing past variations of the main oceanographic and climatic features in the north-central Chilean coast, we analyzed recent sedimentary records of a transitional semi-arid ecosystem susceptible to environmental forcing conditions. Sediment cores were retrieved from two bays, Guanaqueros and Tongoy (29−30°S), for geochemical and biological analyses including: sensitive redox trace elements, biogenic opal, total organic carbon (TOC), diatoms, stable isotopes of organic carbon and nitrogen. Three remarkable periods were established, with different environmental conditions and productivities: (1) > cal BP 6500, (2) cal BP 6500 – cal BP 1700 and (3) cal BP 1700 towards the present (CE 2015). The first period was characterized by a remarkably higher productivity (higher diatom abundances and opal) when a large fluxes of organic compounds was also inferred from the accumulation of elements such as Ba, Ca, Ni, Cd and P in the sediments. At the same time, suboxic-anoxic conditions at the bottoms were suggested by the large accumulation of Mo, Re and U, showing a peak at cal BP 6500 when sulfidic conditions could have been established. This was also identified as the driest interval according to the pollen moisture index, although it could be extended until cal BP 5500. These conditions should be associated to an intensification of the SPSA and a stronger SWW, emulating La Niña-like conditions as has been described for the SE Pacific during the early Holocene, which in this case extends until the mid-Holocene. During most of the second period, lower productivity was observed. However, a small increment was identified between Cal BP 4500 and 1700 although low amounts of diatom (valves g^{-1}) and nutrient-type metal accumulations were observed, contrasting with the first period when high opal accumulations and diatom abundances were synchronized. Oxygen conditions at the bottoms change to an almost stable sub-oxic condition during this time interval. The third period is marked by an intense oxygenation after cal BP 1700, as observed by a change in the accumulation of U, Mo and Re. In Addition, a small productivity rise after cal BP ~130 towards recent times was observed, as suggested by opal accumulations but no increment in diatom abundance. Overall, lower primary productivity, higher oxygenation at bottoms and higher humidity conditions were established after cal BP 6500 and towards the present. We suggest that the oxygenation might be associated with intensified El Niño activity or similar conditions that introduce oxygenated waters to coastal zones by the propagation of waves of equatorial origin. This oxygenation is changing the original extent of the accumulation of elements sensitive to redox changes in sediments, even under the prevalence of high productivity and sub-oxic conditions.

Keywords: paleoproductivity, paleoredox, trace metals, diatoms, opal, organic carbon, Coquimbo, SE-Pacific

1. Introduction

Mean climatic conditions at the SE Pacific are modulated by the dynamic of the Southern Pacific Subtropical Anticyclone (SPSA) and the Humboldt Current System. The SPSA has seasonal, decadal and inter-decadal variability modulating the strength of the southern westerly winds (SWW) and hence the main oceanographic feature of the Eastern boundary margin, the upwelling, influencing the biogeochemical processes related to the inputs of nutrient and biological productivity. Seasonal variations produce periods of intense upwelling when the SPSA is stronger, while the opposite is true when it is weak (Croquette et al, 2007). The coastal wind pattern produced alongshore varies along the SE Pacific showing lower seasonality between 18°−30°S, and producing a semi-permanent upwelling (Pizarro et al., 1994; Figueroa and Moffat, 2000). This system is highly affected by the inter-annual variability imposed by El Niño Southern Oscillation (ENSO), with impacts on the wind intensity. The upwelling brings nutrient-poor waters during the warm phase, while the opposite happens during the cold phase (Ruttland and Fuenzalida, 1991; Blanco et al., 2002). Other climate patterns−namely the Pacific Decadal Oscillation (PDO) and the Southern Annular Mode (SAM)−operate on a much longer time scale (inter-annual, decadal, inter-decadal) modifying the strength and the position of the SWW, and thereby producing cold/warm periods and intense/weak upwelling (Ancapichún and Garcés-Vargas, 2015). In addition, the austral insolation influences the extent of the Antarctic sea ice and the Hadley cell, which act as important forces to the latitudinal displacement of the ITCZ (Inter-tropical Convergence Zone; Kaiser et al., 2008, and reference there in). These fluctuations produce humid and arid conditions along the SE Pacific where the wind's intensity remains the key factor for the upwelling's strength and, therefore, for the supply of nutrients to the photic zone, all of which are required for development of primary productivity.

Off Coquimbo (30°S), there is normally a semi-permanent and intense upwelling forced by local winds, strongly influenced by topographic features (Figueroa and Moffat, 2000) and ENSO variability (Escribano et al., 2004). During El Niño, mean winds alongshore reduce their intensity and the South East Pacific anticyclone weakens. Conversely, during La Niña mean winds alongshore increase their intensity and the anticyclone is reinforced (Rahn and Garreaud, 2013). This has an impact on the upper circulation of the ocean affecting oxygenation and the strength of upwelling. The high productivity that takes place close to the coast during normal periods (Escribano et al., 2004 and references therein) maintains a zone of low dissolved oxygen content along the margin reinforcing the oxygen minimum zone (OMZ). This zone develops along the North and South Pacific Ocean and its intensity, thickness, and temporal stability vary as a function of latitude (Helly and Levin, 2004, Ulloa et al., 2012). To the north (e.g. 21°S) and off Peru, the OMZ occurs permanently, and can extend into the euphotic zone. In the case of northern Chile and southern Peru, there is no significant interface with the benthic environment due to the presence of a narrow continental shelf (Helly and Levin, 2004). The OMZ dynamic off Coquimbo has not been studied in detail, but a seasonal intrusion of low oxygen waters to the coast has been observed (Gallardo et al., 2017). During the 97-98 El Niño event, the oxygenation of bottoms was clearly detected in north (23°S) and south-central Chile (36°S) (Ulloa et al., 2001; Sellanes et al., 2007; Gutiérrez et al., 2006), changing the normal suboxic conditions at the bottom, the normal composition of macrofauna and related geochemical characteristics of the sediments that have implications that persist for many years after the event (Sellanes et al., 2007; Gutiérrez et al., 2006).

These changes in primary productivity and oxygenation at the bottom can be observed in sedimentary records which respond to the amount of organic carbon that has settled on the bottom and to the diagenetic reactions during organic matter remineralization. Trace elements are commonly used as indicators of these processes, observed as element enrichment or depletion. It is driven by organic matter fluxes and redox conditions that modify the original extension of metal enrichment, which depend on the oxygen content during early diagenesis in the upper sediment layers and overlying water (Nameroff et al., 2002; Zheng et al., 2002; McManus et al., 2006; Siebert et al., 2003). Therefore they are a useful tool to establish temporal changes in primary productivity and also to establish changes in the oxygenation at the bottom on sedimentary records.

Our work focuses on the past variations of the environmental conditions deduced from marine sedimentary records of inorganic and organic proxies over the last ~8000 years BP, obtained from a transitional semi-arid ecosystem off central Chilean coast (30°S), close to Lengua de Vaca point, the most relevant upwelling area of Chile's northern margin (Shaffer et al., 1999; Thiel et al., 2007). We considered redox trace element measurements that respond to local hypoxia (U, Mo and Re) as well as nutrient-type elements, which follow the organic fluxes to the sediments (Ba, Ni Cu, P) (Tribovillard, 2006). Additionally, we measured Fe and Mn which play a key role in adsorptiondesorption and scavenging processes of dissolved elements in bottom waters and sediments, and we measured Ca, K and Pb used to assess terrigenous inputs by coastal erosion, weathering and eolian transport, which is also true for Fe and Mn (Calvert and Pedersen, 2007). Ca accumulation depends, in turn, on carbonate productivity and dissolution, which has been used as a paleoproductivity proxy (Paytan, 2008; Govin et al., 2012). We determined the enrichment/depletion of elements to establish the main environmental conditions prevailing during the sedimentation of the particulated material (Böning et al., 2009). In addition, we considered the diatoms assemblages with biogenic opal as a measurement of siliceous export production, TOC and stable isotopes to identify variations in the organic fluxes to the bottoms. Moreover, pollen grains were used to identify environmental conditions based on the climate relationship of the main vegetation formations in North-Central Chile. Based on our records we were able to identify wet/dry intervals, periods with high/low organic fluxes to the sediments related to changes in primary production, and changes in the redox conditions at the bottoms.

2. Study area

The Coquimbo area (29-30°S),− in the southern limit of the northern-central Chilean continental margin−constitutes a border area between the most arid zones of northern Chile (Atacama Desert) and the more mesic Mediterranean climate in central Chile (Montecinos et al., 2016). Here, the shelf is narrow and several small bays trace the coast line.

The Tongoy and Guanaqueros bays are located in the southern edge of a broad embayment between small islands to the north (29°S; Choros, Damas and Chañaral) and Lengua de Vaca Point to the south (30°S) (Fig. 1), protected from predominant southerly winds. Tongoy Bay is a narrow marine basin (10 km at its maximum width) with a maximum depth of ~100 m. To the northeast lies Guanaqueros Bay, a smaller and shallower basin. High wind events evenly distributed throughout the year promote an important upwelling center at Lengua de Vaca Point, developing high biomass along a narrow coastal area (Moraga-Opazo et al., 2011; Rahn and Garreaud, 2013), and reaching maximum concentrations of ~20 mg m^{-3} (Torres and Ampuero, 2009). In the shallow waters of Tongoy Bay, the high primary productivity results in high TOC in the water column allowing for the deposition of fine material to the bottom; TOC rises concurrently with the periods of low oxygen conditions (Fig. 3; Muñoz et al., unpublished data). Recent oceanographic studies indicate that low dissolved oxygen water intrusions from the shelf (Fig. 2) seem to be related to lower sea levels resulting from local wind annual cycles at a regional meso-scale (Gallardo et al., 2017). The spatial and temporal variability of these processes is still under study.

Sedimentological studies are scarce in Chile's northern-central shelf. A few technical reports indicate that sediments between 27°S and 30°S are composed of very fine sand and silt with relatively low organic carbon content (<3 and ~5%), except in very limited coastal areas where organic material accounts for approximately ~16% (Muñoz, unpublished data; FIP2005-61 Report, www.fip.cl). Coastal weathering is the main source of continental input due to scarce river flows and little rainfall in the zone (0.5 to ~80 mm yr^{-1}; Montecinos et al., 2016, Fig.1). Freshwater discharges are represented by creeks, which receive the drainage of the coastal range forming wetland areas in the coast and even small estuaries, such as Pachingo, located south of Tongoy (Fig. 1). These basins cover ~300 and 487 km^2, respectively. The water volume in the estuaries is maintained by the influx of seawater mixed with groundwater supply. No surface flux to the sea is observed. Therefore, freshwater discharge occurs only during high rainfall periods in the coastal zone (DGA, 2011), which normally takes place during El Niño years when higher runoff has been recorded in the area during the austral winter (Valle-Levinson et al., 2000; Garreaud et al., 2009). Under this scenario, marine sediments are often highly influenced by primary production in the water column, and therefore, sedimentary records can reveal past variability in primary production and in the oceanographic conditions over the shelf, which ultimately respond to major atmospheric patterns.

3. Materials and methods

3.1. Sampling

Sediment cores were retrieved from two bays in the Coquimbo region: Bahía Guanaqueros (core BGGC5; 30°09' S, 71°26' W; 89 m water depth) and Bahía Tongoy (core BTGC8; 30°14' S, 71°36' W; 85 m water depth) (Fig. 1.), using a gravity corer (KC-Denmark) during May 2015, on board the L/C Stella Maris II owned by the Universidad Católica del Norte. The length of the cores was 126 cm for BGGC5 and 98 cm for BTGC8.

Subsequently, the cores were sliced into 1-cm sections and subsamples were separated for grain size measurements, magnetic susceptibility, trace elements, biogenic opal, C and N stable isotope signatures ($\delta^{13}C$, $\delta^{15}N$), and TOC analyses. The samples were first kept frozen (–20° C) and then freeze-dried before laboratory analyses.

3.2. Geochronology (^{210}Pb and ^{14}C)

Geochronology was established combining ages estimated from $^{210}Pb_{xs}$ activities suitable for the last 200 years and radiocarbon measurements at selected depths for older ages. ^{210}Pb activities were quantified through alpha spectrometry of its daughter ^{210}Po following the procedure of Flynn (1968). $^{210}Pb_{xs}$ (unsupported) activities were determined as the difference between ^{210}Pb and ^{226}Ra activities measured in some intervals of the sediment column. ^{226}Ra was measured by gamma spectrometry at the Laboratoire Géosciences of the Université de Montpellier (France). Standard deviations (SD) of the ^{210}Pb inventories were estimated propagating counting uncertainties (Bevington and Robinson, 1992) (Table S1, supplementary data). The ages were based on the Constant Rate of Supply Model (CRS, Appleby and Oldfield, 1978).

Radiocarbon measurements were performed on a mix of planktonic foraminifera species in core BGGC5 whereas the benthic foraminifera species *Bolivina plicata* was selected for core BTGC8 (Table 1). The samples were submitted to the National Ocean Sciences AMS Facility (NOSAMS) of the Woods Hole Oceanographic Institution (WHOI). The time scale was obtained according to the best fit of ages obtained from $^{210}Pb_{xs}$ and ^{14}C (Fig. 4), using the CLAM 2.2 software and using the Marine curve 13C (Reimer et al., 2013). A reservoir deviation from the global mean reservoir age (DR) of 441 ± 35 years was considered, established according Sabatier et al. (2010). This was estimated subtracting the 14C age value corresponding at the historical dates 1828 AD and 1908 AD (499 ± 24 and 448 ± 23 ^{14}C yr, respectively, Reimer et al., 2013) from the apparent ^{14}C age of foraminifers measured at depths of 5 and 10 cm for cores BTGC8 and BGGC5, respectively (Sabatier et al., 2010; Table 2).

3.3. Geophysical characterization

Magnetic susceptibility ($SIx10^{-8}$) was measured with a Bartington Susceptibility Meter MS2E surface scanning sensor in the Sedimentology Laboratory at Centro Eula, Universidad de Concepción. Mean values from three measurements were calculated for each sample.

Grain size was determined using a Mastersizer 2000 laser particle analyzer, coupled to a Hydro 2000−G Malvern in the Sedimentology Laboratory of Universidad de Chile.

Skewness, sorting and kurtosis were evaluated using the GRADISTAT statistical software (Blott and Pye, 2001), which includes all particle size spectra.

3.4. Chemical analysis

Trace element analyses were performed by ICP-MS (Inductively Coupled Plasma-Mass Spectrometry) using an Agilent 7700x at Université de Montpellier (OSU OREME/AETE regional facilities). Sediment samples and geochemical reference materials (UBN, BEN and MAG1) were dissolved using a concentrated mix of acids (HF-HNO_3-$HClO_4$) in Savillex screw-top Teflon beakers at 120°C. Final solution considered the addition of a known weight of internal standard solution consisting of 1 ppb of In and Bi. Internal standardization used ultra-pure solution enriched in In and Bi, both elements whose natural abundances in geological samples do not contribute significantly to the added internal standard. This is used to deconvolve mass-dependent sensitivity variations of both matrix and instrumental origin, occurring during the course of an analytical session.

Mean metal concentrations for the analyzed samples were determined by external calibrations prepared daily from multi- and mono-elemental solutions, with concentrations in the range of 0.05−10 ppb for trace elements and of 1−10 ppm for major elements (Ca, K). Polyatomic interferences were controlled by running the machine at an oxide production level <1%. The analytical precisions attained by this technique were between 1% and 3% and accuracy better than ±5%.

TOC and stable isotope ($\delta^{15}N$ and $\delta^{13}C$) analyses were performed at the Institut für Geographie, Friedrich Alexander Universität (FAU) Erlangen-Nürnberg, Germany using a Carlo Erba elemental analyzer NC2500 and an isotope-ratio-mass spectrometer (Delta Plus, Thermo-Finnigan) for isotopic analysis. Carbon and nitrogen contents were determined from the peak-area-versus-sample-weight ratio of each individual sample and calibrated with the elemental standards cyclohexanone-2,4-dinitrophenylhydrazone ($C_{12}H_{14}N_4O_4$) and atropine ($C_{17}H_{23}NO_3$) (Thermo Quest). A laboratory-internal organic standard (Peptone) with known isotopic composition was used for final isotopic calibrations. Stable isotope ratios are reported in the δ notation as the deviation relative to international standards (Vienna Pee Dee Belemnite for $\delta^{13}C$ and atmospheric N_2 for $\delta^{15}N$), so $\delta^{13}C$ or $\delta^{15}N = [(R\ sample/R\ standard) - 1] \times 10^3$, where R is $^{13}C/^{12}C$ or $^{15}N/^{14}N$, respectively. Typical precision of the analyses was ±0.1‰ for $\delta^{15}N$ and $\delta^{13}C$.

Biogenic opal was estimated following the procedure described by Mortlock and Froelich (1989). The analysis was done by molybdate-blue spectrophotometry (Hansen and Koroleff, 1999) conducted at the laboratories of Marine Organic Geochemistry and Paleoceanography, University of Concepción, Chile. Values are expressed as biogenic opal by multiplying the Si (%) by 2.4 (Mortlock and Froelich, 1989). Analytical precision was ± 0.5%. Accumulation rates were determined based on sediment mass accumulation rates and amount of opal at each core section in %.

3.5. Microfossils analyses

Qualitative abundances of siliceous microfossils were carried out every centimeter following the Ocean Drilling Program (ODP) protocol described by Mazzullo et al. (1988), with this information were selected some sections every ~4, 8 and 12 cm for BGGC5 and at ~6 cm for BTGC8 for quantitative abundances of microfossils (diatoms, silicoflagellates, sponge spicules, crysophyts and phytoliths). Briefly ~ 0.5 g of freeze-dried sediment was treated according to Schrader and Gersonde (1978) for siliceous microfossils. Siliceous microfossils were identified and counted under an Olympus CX31 microscope with phase contrast. 1/5 of the slides were counted at 400X for siliceous microfossils and one transect at 1000x was counted for *Chaetoceros* resting spores (*Ch*. resting spores). Two slides per sample were counted; the estimated counting error was 15%. Total diatom abundances are given in valves g^{-1} of dry sediments.

Pollen analysis was conducted following the standard methodology for sediment samples (Faegri and Iversen, 1989). The samples were mounted with liquid glycerol and sealed permanently with paraffin wax. Pollen identification was conducted under a stereomicroscope at 400 fold magnification with the assistance of the Heusser (1973) pollen catalogue. A total of 100-250 terrestrial pollen grains were counted on each sample depending on their abundance. Pollen percentage for each taxon was calculated from the total sum of terrestrial pollen. The percentage of aquatic pollen and fern spores was calculated based on the total terrestrial sum plus their respective group. Pollen percentage diagrams were generated using the Tilia software (E. Grimm, Illinois State Museum, Springfield, IL. USA). The diagram was divided into "zones" based on the identification of the most important changes in pollen percentage and assisted by a cluster ordination (CONISS) performed by the same software.

We further summarize pollen-based precipitation trends by calculating a Pollen Moisture Index (PMI), which is defined as the normalized ratio between Euphorbiaceae (wet coastal scrubland) and Chenopodiaceae (arid scrubland). Thus, positive (negative) values of this index indicate the relative expansion (reduction) of coastal scrubland under relatively wetter (drier) conditions.

4. Results

4.1. Geochronology

$^{210}Pb_{xs}$ (unsupported activity) was obtained from the surface at a depth of 8 cm in the two cores, with an age of ~ AD 1860 at 8 cm in both (Table S1). Greater surface activities were obtained for core BGGC5 (13.48 ± 0.41 dpm g^{-1}) compared to core BTGC8 (5.80 ± 0.19 dpm g^{-1}), showing an exponential decay with depth (Fig. 4). A recent sedimentation rate of 0.11±0.01 cm yr^{-1} was estimated.

The age model provided a maximum age of cal BP 8210 for core BGGC5, and cal BP 7941 for core BTGC8 (Fig. 4). A mean sedimentation rate of 0.02 cm yr^{-1} was estimated for core BGGC5, with a period of relative low values (0.01 cm yr^{-1}) between cal BP ~4000 and 6000. For BTGC8, sedimentation rates were less variable and around 0.013 cm yr^{-1} in the entire core. An age reserve estimation following the method by Sabatier et al. (2010) resulted in 441 ± 35 and 442 ± 27 years for BGGC5 and BTGC8 cores, respectively (Table 2). These values were close to the global marine reservoir and higher than other estimations along the Chilean margin at shallower depths (146 ± 25 years at < 30 water depth; Carré et al., 2016; Merino-Campos et al., 2018). Our coring sites are deeper (~90 m water depth) and influenced by upwelled water from Lengua de Vaca Point, which could explain such differences. However, moderate differences were observed between models using both reservoir values. Thus, our estimations were based on two pre-bomb values established with ^{210}Pb measured in sediments and ^{14}C in foraminifers, used for the age modeling.

4.2. Geophysical characterization

Sediments retrieved from the bays showed fine grains within the range of very fine sand and silt in the southern areas. There, grain size distribution was mainly unimodal, very leptokurtic, better sorted and skewed to fine grain when compared to sediments from the northern areas. Sediment cores obtained from the northern areas were sandy (coarse sand and gravel), with abundant calcareous debris. Longer cores of soft sediment were retrieved at the southernmost areas (BGGC5 and BTGC8), where the silty component varied between 40 % and 60 % (Fig. 1 and 5a,b). The clay component was very low at both cores (<2%). The sediment's color ranged from very dark grayish brown to dark olive brown (2.5Y 3/3−3/2) in Guanaqueros Bay (BGGC5) and from dark olive gray to olive gray (5Y 3/2−4/2) in Tongoy Bay (BTGC8). Visible macro-remains (snails and fish vertebrae) were found, as well as weak laminations at both cores. The magnetic susceptibility showed higher values close to the surface, up to 127 SI x10^{-8} at BGGC5, and relative lower values (85 SI x10^{-8}) at BTGC8. At greater depths, however, the values were very constant, around 5−8 x10^{-8} SI at BGGC5 core and around 12−20 x10^{-8} SI at BTGC8 core. In both cores, susceptibility rises substantially in the last century (Figs. 5a, 5b). Lower bulk densities were estimated at core BGGC5 (0.7−0.9 g cm^{-3}), compared with core BTGC8 (>1 g cm^{-3}) (Fig. 5a, 5b). In line with this, mean grain size amounted to 60−80 µm in Guanaqueros Bay (BTGC8), compared to 50−60 µm in Tongoy Bay (BGGC5). Both cores were negatively skewed, with values of -1 to -1.2 at BGGC5, and -1 to -2.5 at BTGC8. Minor increases towards coarser grain size were observed in the last ~1000 years, especially in Tongoy Bay (BTGC8). In both cases, grain size distributions were strongly leptokurtic. Ca/Fe ratio also reduced in time, except at core BTGC8 where it was only observed during the last ~2000 years.

4.3. Biogenic components

4.3.1. Siliceous microfossils and biogenic opal

Total diatom abundance fluctuated between 5.52 x10^5 and 4.48 x10^7 valves g^{-1} at core BGGC5. Total diatom abundance showed a good correlation with biogenic opal content at BGGC5 (R^2 =0.52, P<0.5), with values raising from 72 cm to the bottom of the core, corresponding to cal BP 5330, and reaching their highest values before cal BP 6500. On the contrary, diatom abundance and biogenic opal were much lower at core BTGC8 (< 2 $\times 10^5$ valves g^{-1} and <3%, respectively). Here, the siliceous assemblage was almost completely conformed by *Chaetoceros* resting spores (RS) (Fig. 6).

A total of 135 and 8 diatom taxa were identified in cores BGGC5 and BTGC8 respectively, where core BTGC8 registered very low diatom abundances. In general, diatoms were the most important assemblage of siliceous microfossils (96 %), followed by sponge spicules (3 %). The contribution of phytoliths and chrysophyte cysts was less than 2 % at core BGGC5. *Chaetoceros* (RS) dominated diatom assemblage (~90 %; Fig. 6), and included the species *C. radicans, C. cinctus, C. constrictus, C. vanheurckii*, *C.*

coronatus, *C. diadema*, and *C. debilis*. Other upwelling group species recorded (mainly at core BGGC5) were: *Skeletonema japonicum,* and *Thalassionema nitzschioides* var. *nitzschioides* (Table S2). Freshwater diatoms (*Diploneis papula, Cymbella tumida, Fragilaria capucina, Diatoma elongatum)* and non-planktonic diatoms (*Cocconeis scutellum, C. costata and Gramatophora angulosa*) accounted for ~0.1−5 %; while the group of coastal planktonic diatoms accounted for ~0.3−6 % of the total assemblage. The main planktonic diatoms were (*Rhizosolenia imbricata*, and *Thalassiosira eccentrica*). Oceanic-warm diatoms (*Roperia tesselata*, *Th. nitzschioides var inflatula)* and the tycoplanktonic diatom group were rare, with less than 1 %.

4.3.2. TOC and stable isotopes distribution

Consistent with opal and diatoms, core BGGC5 showed higher values of TOC (between 2 % and 5 %) compared with less than ~1.5 % at core BTGC8 (Fig. 5a,b). Furthermore, $\delta^{13}C$ was slightly higher at core BTGC8 (-20 ‰ to -21 ‰) compared with core BGGC5 (-21 ‰ to -22 ‰), the former is also showing slightly higher values of $\delta^{15}N$ from the deeper sections to the surface of the core (<7 ‰ to >10 ‰). This increase was less evident at core BGGC5, with values of ~9 ‰ at depths to >10 ‰ on the surface (Fig. 5a,b). The reduced TOC content was related to slightly higher $\delta^{13}C$ values (~ -20 ‰) in both cores.

4.3.3. Pollen record

Initial surveys at core BTGC8 (Tongoy Bay) revealed extremely low pollen abundances which hampered further palynology work. A comprehensive pollen analysis was only conducted for core BGGC5 (Guanaqueros Bay). The pollen record of core BGGC5 consisted of 29 samples shown in Figure 7. The record was divided into five general zones following visual observations of changes in the main pollen types and also assisted by CONISS cluster analysis.

Zone BG-1 (cal BP 8200 – 7600): This zone is dominated by the herbaceous taxa Chenopodiaceae, *Leucheria*-type, Asteraceae subfamily (subf.) Asteroideae, Apiaceae with overall high values for the wetland genus *Typha* spp.

Zone BG-2 (cal BP 7600 – 6500): This zone is also dominated by Chenopodiaceae, *Leucheria*-type and Asteraceae subf. Asteroideae. In addition, other non-arboreal elements such as *Ambrosia*-type, Poaceae, Brassicaceae and *Chorizanthe* spp. expand considerably.

Zone BG-3 (cal BP 6500 –3400): This zone is marked by a steady decline in Chenopodiaceae and *Leucheria*-types, and by the expansion of several other herbaceous elements, such as Euphorbiaceae, *Baccharis*-type and Brassicaceae.

Zone BG-4 (cal BP 3400 – 120): This zone is mostly dominated by Ast. subf. Asteroideae, and marked by the decline of Chenopodiaceae and *Leucheria*-type. Other coastal taxa –such as Euphorbiaceae, *Baccharis*-types, Asteraceae subf. Chichorioideae, *Quillaja saponaria*, Brassicaceae and *Salix* spp.– also expand in this zone.

Zone BG-5 (cal BP 120 – -60): The upper portion of the record is dominated by Asteraceae subf. Asteroideae and Poaceae, and marked by higher amounts of Geraniaceae, Asteraceae subf. Mutisieae, Myrtaceae and *Q. saponaria*. Additionally, this zone includes introduced pollen types such as *Rumex* spp. and *Pinus* spp. The latter is not shown in the diagram of Figure 8 because its abundance was minimal.

Overall, the most distinctive trend revealed by core BGGC-5 is a long-term reduction in Chenopodiaceae and higher amounts of Euphorbiaceae and Asteraceae subf. Asteroideae. Along with these changes, a further expansion of several other pollen representative of the coastal shrub land vegetation began at about cal BP 6500.

4.4. Trace element distributions

Trace element distributions are shown in figures 8a and 8b for Guanaqueros (BGGC5) and Tongoy Bays (BTGC8), respectively. We use Al as a normalizing parameter for enrichment/depletion of elements due to its conservative behavior. The elements are presented as metal/Al ratios. Trace metals are sensitive to the presence of oxygen (U, Re, Mo) showing an increasing metal/Al ratio from the base of core BGGC5 (cal BP ~8210) up to cal BP 6500. After this peak, ratios showed a slight increase towards cal BP 1700, close to the beginning of the recent era, followed by a sharp reduction until present. Similarly, metal ratios at core BTGC8 increase over time, yet the peak was observed at cal BP ~1000. The exception to this trend was Mo, which reached a maximum value up to cal BC 6500 and then reduced steadily into the present. Additionally, metal/Al values were higher at core BGGC5. Iron revealed a clear upward trend around cal BP 3300 − 3500 at core BGGC5, which was not clearly observed at the Tongoy core. Instead, core BTGC8 showed peak Fe values around cal

BP 6500 – 7800; in both cores Fe increased in the past 130 years. No clear trend could be established for Mn.

A second group of elements (metal/Al ratios), including Cd, Ni and P (related to primary productivity and organic fluxes), showed a pattern similar to that of Mo/Al towards the bottom of core BGGC5, i.e. increasing values from cal BP ~8000 reaching highest values around cal BP 6500; after that the values followed constant reductions towards the present. A third group, consisting of Ba, P and Ca, exhibited a less clear pattern. Cd/Al and Ni/Al ratios at core BTGC8 showed only slightly decreasing values, and very low peak values compared to core BGGC5. The same pattern is observed for other elements. Metal/Al ratios for Ba, Ca and P were lower and presented a long-term reduction pattern towards the present.

An exception to the previously described patterns was Cu/Al, which reach a maximum value at cal BP ~3600 –3700 and showed a conspicuous upward trend in the past ~130 years. This was also observed at core BTGC8, but with lower concentrations than at core BGGC5.

The authigenic enrichment factor of elements was estimated according to: EF = $(Me/Al)_{sample}$ / $(Me/Al)_{detrital}$; where $(Me/Al)_{sample}$ is the bulk sample metal (Me) concentration normalized to Al content and the denomination "detrital" indicates a lithogenic background (Böning et al., 2009). Detrital ($[Me]_{detrital}$ and $[Al]_{detrital}$) concentrations were established considering local TM abundance, which is more accurate than using mean Earth crust values (Van der Weijden, 2002). We used average element concentrations on surface sediments (0–3 cm) of the Pachingo wetland (Table 3). The values suggest a large enrichment of nutrient-type elements in a period prior to Cal BP 6500, following the trend of the Me/Al ratios, except for Ba and Fe which did not show authigenic enrichment. EFs showed a sharp enrichment reduction at recent time after Cal BP 130 (Table 4).

5. Discussion

5.1. Sedimentary composition of the cores: terrestrial *versus* biogenic inputs

The sediments in the southern zones of the bays are a sink of fine particles transported from the north and the shelf (Fig. 5a, 5b), and respond to water circulation in the Guanaqueros and Coquimbo Bays (Fig. 1). Both have been described as bipolar, i.e. two counter-rotating gyres moving counterclockwise to the north and clockwise to the south (Valle-Levinson and Moraga, 2006). This is the result of the wind's predominant direction and a coastline shape delimited by two prominent points to the north and south. Circulation in Tongoy Bay (the southernmost bay of the system) shows a different pattern due to its northern direction compared to Guanaqueros Bay, which opens to the west. The cyclonic recirculation in Tongoy Bay seems to be part of a gyre larger than the Bay's circulation (Moraga-Opazo et al., 2011) (Fig. 1). This could explain the differences in the distribution and composition of sediment particles between both Bays. In Tongoy Bay, there is less organic carbon accumulation (< 3 g m^{-2} yr^{-1}), siliceous microfossils and pollen (Figs. 5b, 6 and 7). Similarly, in Guanaqueros Bay TOC contents are only slightly higher (> 2 %), especially between cal BP 3700 and 4000 and before cal BP 6500 (~ 4 %), but with greater accumulation rates of about 7 and 16 g $m^{-2}yr^{-1}$, respectively (Fig. 5a). However, these sediments contain enough microfossils to establish differences in primary productivity periods and also provide a pollen record evidencing prevailing environmental conditions.

Stable isotopes measured in the study area were in the range of marine sedimentary particles for southern oceans at low and mid-latitudes ($\delta^{13}C$; -20 ‰ – -24 ‰; Williams 1970; Rau et al., 1989; Ogrinc et. al. 2005), and slightly lower than the TOC composition in the water column (-18 ‰, Fig. 3). This suggests that the organic particles that settle on the bottom are a more refractory material (C/N: 9−11), remineralized during particle transportation and sedimentation. This results in lighter isotopic compositions, especially at core BTGC8. Furthermore, $\delta^{15}N$ and $\delta^{13}C$ in settled particles have higher negative values in surface sediments due to a preferential decomposition of molecules rich in ^{13}C and ^{15}N, resulting in lighter isotope values and higher C/N ratios in sediments than in suspended particles (Fig. 3, 5a, 5b). However, this is also due to the stronger diagenetic reactions observed near the bottom layer (Nakanishi and Minagawa, 2003). Thus, these sediments are composed by winnowed particles transported by water circulating over the shelf, and the isotopic variations should not clearly establish the contribution of terrestrial inputs.

Otherwise, the isotopic composition of upwelled NO_3^- (De Pol-Holz et al., 2007) could influence the variability of $\delta^{15}N$. Values for $\delta^{15}N$ in northern and central Chile are in the range of those measured at the BGGC5 core (~11 ‰; Hebbeln et al., 2000, De Pol-Holz et al., 2007), resulting from the isotopic fractionation of NO_3^- during nitrate reduction within OMZ, leaving a remnant NO_3^- enriched in ^{15}N (Sigman et al., 2009; Ganeshram et al., 2000 and references therein). In this case, BGGC5 core sediments represent the effect of the upwelling's nutrient supply and the influence of OMZ on the shelf, resulting in $\delta^{15}N$ of 9 – 10 ‰. At sediment core BTGC8, lower values (< 8 ‰) measured at greater depths within the core should account for the mix with isotopically lighter terrestrial organic matter (Sweeney and Kaplan, 1980) due to its vicinity to a small permanent wetland in the southern side of Tongoy Bay. The material collected at Pachingo wetland showed $\delta^{15}N$ of 1 – 8 ‰ (Muñoz et al., data will be published elsewhere) in the range of sedimentary environments influenced by terrestrial runoff (Sigman et al., 2009). Likewise, in most cases lower TOC is consistent with lighter isotope $\delta^{15}N$ values, and also with higher C/N ratios, suggesting a combination with continental material (Fig. 5b).

MS measurements revealed lower values in both cores (BGGC5: 5 – 8 $x10^{-8}$ SI; BTGC8: 12 – 20 $x10^{-8}$ SI), except during the last ~200 years (CE 1800), when it reaches higher values substantially similar to those observed in the Pachingo wetland (40 – ~200 x 10^{-8} SI; unpublished data), in the southern area of Tongoy Bay, pointing to an increase in flooding events in the last 200 years. Magnetite has a strong response to magnetic fields and its concentration is considered proportional to magnetic susceptibility (Dearing, 1999), but suffers post-depositional transformations (alteration of magnetite minerals) and can be diluted by biogenic components (carbonates, silicates), altering the MS intensity in areas with high organic accumulation rates (Hatfield and Stoner, 2013). This, however, is not the case of our cores where low sedimentation rates were estimated (0.01 – 0.02 cm yr^{-1}) and the MS should be mainly accounting for the particles' source. The higher MS measurements on surface sediments would indicate a greater contribution of terrestrial material. The area is surrounded by several creeks that are only active during major flooding events, with greater impacts on Tongoy compared to Guanaqueros Bay. There has been a considerable increment in the contribution of terrigenous material in Tongoy Bay, in recent times (Ortega et al., 2019), which is diluting organic proxy records and increasing the grain size. Our records indicate a slight increase in mean grain size in both bays, supported also by a slight reduction in the Ca/Fe ratio pointing to a higher Fe input from continental erosion (Fig. 5a, 5b). Furthermore, lower concentrations of Ca in the deepest part of both cores to the surface was interpreted as a declining primary productivity (Keshav and Achyuthan, 2015; Sun et al., 2016); however, higher concentrations were measured in core

BGGC5 compared with core BTGC8, where more terrigenous influence is being suggested. The slight rise of K/Ca ratio in time –from the bottom to the surface– should also be interpreted as a slight growth of the continental input, since K is related to siliciclastic material from coastal erosion, and from fluvial and groundwater inputs. However, the variation of Ca was larger (Fig.6a, 6b), resulting in higher K/Ca ratios on the surface. This suggests that the continental input has not changed much in time –at a millennial scale– but rather that primary productivity has declined (Fig. 5a, 5b).

Thus, cores BGGC5 and BTGC8 in Guanaqueros and Tongoy Bays are recording the variability of oceanographic conditions, but in the Tongoy core, the concentration of oceanographic proxies dilute due to the input of terrigenous material. This helps to decipher the climatic variability considering that the main input of clastic material to the area takes place during major flooding events. Additionally, the main circulation of the bay system leads to favorable conditions for sedimentation and the preservation of organic marine proxies in the Guanaqueros Bay, hence making the sedimentary records of these sites complementary.

5.2. Temporal variability of proxies for primary productivity

Several elements that take part in phytoplankton growth are useful to interpret the variations in primary productivity with time, as they are preserved in the sediments under suboxic-anoxic conditions. This produces enrichment over crustal abundance which distinguishes them from continental inputs. The presence of free dissolved sulfides produced by sulfate reduction reactions in the diagenesis of organic matter allows for the precipitation of metals into pore waters (Calvert and Pedersen, 1993; Morse and Luther, 1999). At the same time, organic matter remineralization releases ions into pore waters where they could form organic complexes and insoluble metal sulfides. Conversely, they could be incorporated into pyrite as Cd, Ni and Cu, showing different degrees of trace metal pyritization (Huerta-Diaz and Morse, 1992). Ca, Sr, Cd and Ni profiles suggest a lower share of organic deposition over time (Fig. 8a, 8b), consistent with the slight reduction of TOC content observed in the sediments (Figs. 5a, 5b), and concomitantly with other elements related to organic fluxes to the bottom and primary productivity. In the case of Ba, it is actively incorporated into phytoplankton biomass or adsorbed onto Fe oxyhydroxides, increasing the Ba flux towards the sediments, where it is also released during organic matter diagenesis. Ba is precipitating in microenvironments where Ba-sulfate reaches supersaturation (Tribovillard et al., 2006 and references therein), but it is dissolved in suboxic-anoxic environments or where sulfate is significantly depleted (Torres et al., 1996; Dymond et al., 1992). Therefore, it is better preserved in less anoxic environments with moderate productivity, expected to be the case of our study site (Gross Primary Productivity =0.35 to 2.9 g C $m^{-1}d^{-1}$; Daneri et al., 2000). Hence, the slight rise of Ba from cal BP 4000 to the present (Fig. 8a) is more of a response to a less anoxic environment than to an increase in primary productivity, and results in a low negative correlation with TOC (-0.59; Table 5) due to Ba remobilization in anoxic conditions before cal BP 6500. After this age, the reduction in TOC and other nutrient-type elements (Ni, Sr, Ca, Cd) into the present is consistent with the rise in oxygen in bottoms. On the other hand, P distribution showed a trend similar to that of TOC and other elements related to organic fluxes into the bottom (Ni, Cd), although with a lower correlation (~0.6). The accumulation of P depends on the deposition rate of organic P (dead plankton, bones and fish scales) on the bottom, and is actively remineralized during aerobic or anaerobic bacterial activity. P and TOC showed a declining trend towards the present, suggesting reducing flux of organic matter over time, which was also observed for Ni and Cd distributions. Alternatively, reducing fluxes of organic proxies could be explained by the higher remineralization of organic material settled on the bottom due to higher oxygen availability (Figs. 8a, 8b).

Productivity reconstructions were based on qualitative diatom and sponge spicules relative abundances, quantitative diatom counts (valves g^{-1}) and biogenic opal content only in core BGGC5, since core BTGC8 registered low valve counts (< 1 % in relative diatom abundance). However, in both cores diatom assemblages were represented mainly by *Ch.* resting spores, which are used as upwelling indicators, showing higher concentrations during periods of high productivity and upwelling (Abrantes 1988, Vargas et al., 2004). In addition, *Ch.* resting spores are highly silicified and well preserved in coastal sediments (Blasco et al., 1981). The downcore siliceous productivity based on opal distribution (Fig. 6) distinguished three main time intervals of higher productivity: (1) > cal BP 6500, (2) cal BP 1700 – cal BP 4500 and (3) recent times (CE 2015) – cal BP ~130. The opal accumulation rate in the first interval was remarkably high, amounting to ~27 ± 13 g m^2 yr^{-1} (range: 9 – 53 g $m^{-2}yr^{-1}$, Table 4), when *Chaetoceros* spores were predominant, indicating an upwelling intensification; during the second interval, it decreased to ~ 11 ± 4 g m^2 yr^{-1} (range: 2 –

21 g $m^{-2}yr^{-1}$, Table 4). This is partially consistent with nutrient–type element distributions (Fig. 8a). The third interval accounts for the last ~200 years, when high opal accumulations and high Cd/U ratios could also be observed increasing towards the present (mean opal value of 29 ± 14 g m^2 yr^{-1}, range: 3 – 40 g m^2 yr^{-1}). However, low diatom abundances were observed (range: 0.5 – 4.9 $x10^6$ valves g^{-1}), probably because recent sedimentation rates were higher, altering the estimations of opal flux. Additionally, few sections of the core surface were analyzed for diatoms leading to a low resolution of this measurement in the most recent period. Cu and Fe also increased during this period (Fig. 8a), contributing to fertilize the environment and promoting primary productivity. In this sense, higher productivity in the last 200 years could be suggested but further investigations are needed. The second time interval with a higher productivity was not clearly identified in terms of metals, except for Fe, which clearly shows higher values during this period (Fig. 8a). During the first period, all metal proxies showed primary productivity increases before cal BP 6500, as indicated by opal accumulation within the sediments. Here, Cd and U accumulations in the sediments resulted in high Cd/U ratios, even at core BTGC8 (> 2; Fig. 6), indicating very low oxygen conditions (Cd/U ratios could vary between 0.2 and 2 from suboxic to anoxic environment; Nameroff et al., 2002). Lower ratios (< 1; Fig. 6) were estimated when the opal accumulation was low during the second time interval, indicating higher variations in primary productivity over time with moderate changes in oxygen conditions in the bottoms. Furthermore, opal showed good correlations with Ni and Cd (˜0.70; Table 5; Fig. 8a), all of which suggests the relevance of bottom organic fluxes for the buildup of elements within the sediments, and establishes a clear period of higher primary productivity around cal BP 6500, when the lowest oxygen conditions prevailed (Fig. 6).

5.3. Temporal variability of proxies for bottom water oxygenation

The distributions of U, Re and Mo at core BGGC5 indicate that anoxic or suboxic conditions were developed from cal BP 8200 to ~ cal BP 1700 (Fig. 8a, 8b). After this period and into the present, however, a remarkable reduction in their concentration suggests a more oxygenated bottom environment, concurrent with lower organic fluxes to the sediments. The Re profile shows the influence of suboxic waters not necessarily associated with higher organic matter fluxes to the bottom. Since this element is not scavenged by organic particles, its variability is directly related to oxygen changes (Calvert and Pedersen, 2007, and references therein). Additionally, it is strongly enriched above crustal abundance under suboxic conditions (Colodner et al., 1993; Crusius et al 1996), being >10 times at core BGGC5 (Table 4) before cal BP 1700. Similarly, U shows a similar pattern and while organic deposition has an impact on its distribution (Zheng et al., 2002), it is also related to changes in bottom oxygen conditions. This is because its shift from a soluble conservative behavior to a non-conservative and insoluble behavior depends solely on redox potential changes that occur near the Fe(III) reduction zone (Klinkhammer and Palmer, 1991.). Molybdenum, which showed higher values at cal BP 6500, also indicates the presence of sulfidic conditions, as shown by a Re distribution highly enriched under anoxic environments (Colodner et al., 1993), and by the reduction of Re(VII) to Re(IV), forming ReO_2 or ReS (Calvert and Pedersen, 2007). The enrichment of Rhenium, U and Mo is used to decipher the redox condition within the sediments, even in places with high lithogenic inputs that could obscure the authigenic enrichment of other elements under similar conditions (Crusius et al., 1996). In both places, the concentrations of these elements showed values above the crustal abundance, especially in core BGGC5 (Table 4), with Re and Mo enriching by ~19 and U by ~5, except in the past ~1700 years when they reduced by half. This suggests that the presence of anoxic conditions was stronger before cal BP 1700 (based on mean EFs and Me/Al ratios distribution), with a peak around cal BP 6500 (based on EF_{Cd}) and followed by a less anoxic condition after cal BP ~1700 (Fig. 8a, Table 4). The most important enrichment was observed for Cd (> 30) that was higher before cal BP 6500 (~140), in agreement with higher opal accumulation and diatom abundance (Fig. 6, Table 4). The most important enrichment could similarly indicate the sulfidic condition within the sediments that allows for Cd precipitation. It is also supported by Mo enrichment (mean EF_{Mo}=16.9), since its buildup within the sediments is highly controlled by sulfide concentrations (Chaillou et al., 2002; Nameroff et al., 2002; Sundby et al., 2004).

Something similar occurs in Tongoy Bay (core BTGC8), but trace metal concentrations are lower for all elements and also for TOC, suggesting a limited influence on metal accumulation within the sediments.

Thus, these elements suggest anoxic or even sulfidic conditions within the sediments in both places at around cal BP 6500 − 7200 (Fig. 8a, 8b). After this period, a second peak but less intense low oxygen condition is observed at the beginning of the recent era (cal BP 1700), continuing with conspicuous oxygenation until present times. This interpretation –based on the distribution of U, Re and Mo– complements the observations of nutrient-type elements pointing both to oxygenation changes and to changes in organic fluxes throughout the sediments. A less prominent accumulation of nutrient-type elements (Ni, Cd, Ba, Ca and P) would point to lower organic matter deposition into the sediments but still promoting low oxygen conditions within the sediments and lower sulfide content over time, which are nevertheless high enough to sustain Mo accumulation until cal BP 1700. After that, lower Re, U and Mo accumulation and EFs were observed, suggesting the relevance of bottom oxygenation (Table 4). This could also explain the conspicuous upward trend of Cu/Al and Fe/Al in recent times due to the presence of oxides (Fig. 8a, 8b). Apparently, a low level of dissolved Cu is maintained by the complexation with organic compounds produced by phytoplankton and Cu adsorption on Fe oxides (Peacock and Sherman, 2004; Vance et al., 2008; Little et al., 2014), with both processes augmenting Cu in the particulate phase over surface sediments (EF_{cu}=4.6±0.5, Table 4). In our study sites, Fe and Cu concentrations were higher in surface sediments, probably related to a higher availability of Fe and Cu in the environment (Fig. 8a, 8b). In turn, this could be associated with mining activities carried out in the area since the beginning of cal BP 14 (AD 1936).

At present, the suboxic conditions inside the Bays result from the influence of adjacent water masses with low oxygen contents related to the oxygen minimum zone (OMZ) (Fig. 2). These suboxic conditions are centered at ~250 m outside the Bays and keep low oxygen concentrations below 40 m within the Bays. Oceanographic time series indicate that transition times develop in short periods due to changes in the directions and intensities of the winds along the coast, which favors upwelling and thus the entry of water with low oxygen content to the Bays with a strong seasonality (http://www.ceazamet.cl/index.php?pag=mod_estacion&e_cod=BTG). Additionally, oceanic variability along the western coast of South America is influenced by equatorial Kelvin waves on a variety of timescales, from intra-seasonal (Shaffer et al.,1997) and seasonal (Pizarro et al., 2002; Ramos et al., 2006) to inter-annual (Pizarro et al., 2002; Ramos et al., 2008). Coastal-trapped Kelvin waves originating from the equator can propagate along the coast, modifying the stability of the regional current system and the pycnocline, and triggering extra-tropical Rossby waves (Pizarro et al., 2002; Ramos et al., 2006; 2008). This oceanographic feature will changes the oxygen content within the bays with major impacts on redox-sensitive elements in surface sediments; thus, the increased frequency and intensity of this variability would result in a mean effect which is observed as a gradual change in metal contents over time.

5.4. Climatic interpretations

The present-day climate of the semi-arid region of Chile is largely influenced by the position of the Southeast Pacific Subtropical Anticyclone (SPSA) and latitudinal displacements of the Southern Westerly Winds (SWW). The dynamic of these large-scale atmospheric systems, from seasonal to decadal timescales, controls the amount of precipitation that reaches this region. Because the semi-arid region of Chile represents the northernmost area under the influence of the SWW, precipitation is relatively scarce and restricted to the austral winter months when SPSA and SWW shift northwards, bringing precipitation fronts to the semiarid coast and inland (Montecinos and Aceituno, 2003; Quintana and Aceituno, 2012).

According to modern climatology, paleoenvironmental records from the semiarid region have mostly been interpreted to reflect past variability in the intensity and latitudinal position of the SWW (Veit et al., 1996; Hebbeln et al., 2002; Lamy et al., 1999; Maldonado and Villagrán, 2002), controlled by the temperature gradient of the ocean's surface (Lamy et al., 2010), sun variability and orbital forcing (Varma et al., 2012; Koffman et al., 2014). Thus, at mid-latitudes of the southern hemisphere, early Holocene has been described as a warm period with summer-like conditions, due to reduced westerlies in the northern margin associated with a reduced sea surface temperature gradient between the tropical and subtropical Pacific (Lamy et al., 2010); period that can be extended until cal BP ~8600−5000 (Kaiser et al., 2008; Ortega et al., 2012, Maldonado et al., 2016). In particular, pollen records from the southern coastal areas of Coquimbo (32°S) point to prevailing wet conditions before cal BP 8700, which brought the expansion of swamp forests areas along the coast followed by a lengthy arid phase until Cal BP 6200 (Maldonado and Rozas, 2008; Maldonado and Villagrán, 2006). This scenario occurred concomitantly with reduced rainfalls and intense coastal humidity associated to coastal fogs that frequently occur during the spring by a strengthening of the SE Pacific Subtropical Anticliclone (Vargas et al., 2006; Garreaud et al 2008; Ortega et al., 2012). This matches the driest conditions along the entire record, detected in the first portion of our pollen reconstruction from core BGGC5 in the Guanaqueros Bay (cal BP 8200 – 7600), still suggesting drier but less intense conditions until cal BP ~5500. This is represented by relatively low values of the Pollen Moisture Index (Fig. 9). The enhancement of regional precipitation has been observed after this date in pollen records in the northern margin of SWW (Jenny et al., 2003; Maldonado and Villagrán, 2006). These findings are also consistent with our Al and Pb records, elements that are usually considered to be indicators of continental particles that enter marine waters by fluvial or aerial means (Calvert and Pedersen, 2007; Govin et al., 2012; Ohnemus and Lam, 2015; Saito et al., 1992; Xu et al., 2015). The trends are similar to the pollen record, i.e., a gradual rise over time, more clearly from cal BP ~5000, suggesting enhanced humid conditions during recent periods (Fig.9). This is also supported by grain size and K/Ca and Fe ratios, known to be indicators of the changes in terrigenous inputs off the coasts in northern-central Chile (Kaiser et al., 2008). Such increments over the last ~5000 years point to higher continental inputs most probably caused by frequent or heavier rainfall events over time, which at present are an important source of sands and K in the northern Chilean margin. K/Ca and Fe distributions point to a mean trend towards more humid conditions, consistent with pollen records at a regional scale (Maldonado & Villagrán 2006); these suggest more humid conditions from cal BP 5000 with the highest values since cal BP 1700. Furthermore, a trend towards increasing precipitations is also consistent with the occurrence of alluvial episodes since cal BP 8600 (Ortega et al., 2012), which following an increasing trend from the mid-Holocene toward recent times (Orthega et al., 2019).

The synchronicity of our records between highest productivity and dry conditions that peak prior to ~cal BP 6500 highlights the role of the SPSA as an important driver of paleoproductivity changes in the coast of semi-arid Chile which prevailed during the early portion of the Holocene to the mid-Holocene (considered as cal BP ~6000). The prevalence of ENSO cold periods between 6700 – 7500 years ago (Carré et al., 2014) or El Niño weak periods between ~4500 and 8000 ka (Rein et al., 2005) are described for the Peru margin, which is consistent with our records and points to more favorable conditions for upwelling strengthening. After this period, a consistent pattern of increasing humidity and continental discharge over the last ~6000 – 5000 years is suggested by our pollen and trace element records. The driver of this long-term paleo-climatic trend seems to be associated with a weak SPSA and a northern position of the SWW, leading El Niño-like conditions. However, lower ENSO variability has been reported at cal BP 4000 – 6000 (Koutavas and Joanides, 2012). Others point to cal BP

4500 (Carré et al., 2014), which does not match our records. The conditions reported by these authors resemble cold periods similar to La Niña-like conditions favorable for upwelling and productivity enhancement, and drier conditions than those recorded during former periods. Therefore, the subsequent weakening in paleo-productivity proxies in our records after cal BP 6500 is not consistent with this scenario. By contrast, a small rise in diatom abundance and opal between cal BP 4500 and 1700, along with the buildup of Ni, Cd and Ca concentrations (Fig. 8), and small increments in organic carbon flux and Cd/U (Fig. 5, 6) suggest higher organic flux and productivity but lower than what was previously observed during cal BP 6500. The slight rise in productivity indicates a weak upwelling that could be explained by a higher frequency of warm events when the modern ENSO regime was established between cal BP ~3000 – 4000 (Carré et al., 2014). In this case, Fe increments could play a role in nutrient inputs for phytoplankton. This has been documented to provide a boost in the primary productivity discussed in the sedimentary records of the northern Chilean margin (Dezileau et al., 2004). In our cores, a short-term rise in Fe concentrations is observed between cal BP ~4000 – 3300 at the Guanaqueros core, whereas persistent high values are recorded in the Tongoy core between cal BP 6500 – 7800. Both of these rises match periods with relatively high primary productivity based on diatoms and opal distributions (Figs. 6, 8b), which supports the role of Fe as a driver of coastal productivity in the past. Additionally, it indicates that an enhanced productivity not only depends on the upwelling's strength but on the availability of nutrients, since this area shows permanent upwelling. In this sense, in periods before cal BP 6500 productivity seems to be controlled mostly by upwelling in more stable climatic conditions, after which local nutrient inputs play a very important role in the development of primary productivity.

In sum, our records show a regular rise in humid conditions concurrently with a declining productivity trend over time after Cal BP 6500. Relevant changes in oceanographic conditions were observed after cal BP 1700, when oxygenation conditions changed drastically at the bottoms, but no such intense change in productivity was observed. Studies of coastal upwelling on the central Peruvian and south central Chilean coasts (12 − 36 °S) reveal that present-day wet/dry variability associated with El Niño Southern Oscillation have a strong impact on bottom ocean oxygenation (Escribano et al., 2004; Gutiérrez et al., 2008; Sellanes et al., 2007). In this regard, OMZs are expected to be less intense during warm El Niño phases and vice versa. This connection has been observed by recent studies, as warm events in the

Tropical Pacific tend to be associated with low productivity and weak OMZ in the Peruvian coast (Salvatteci et al., 2014)

In this case, warm events in the Eastern Pacific could have reduced the ocean's productivity and the organic fluxes resulting from primary productivity, leading to a reduction in oxygen consumption during the diagenesis of organic matter. In the light of these mechanisms, our results suggest more El Niño-like conditions during the latter part of the Holocene –as has been documented for the SE Pacific (Koutavas et al., 2006, Carré et al., 2014)– in agreement with pollen moisture index records and metals described above. According to our records, low oxygen conditions are revealed by higher Mo, Re and U buildup –and sulfidic conditions when Cd is also higher. On the contrary, higher oxygenation should reduce their accumulation in sediments. Thus, more frequent El Niño events during the latter part of the Holocene should be consistent with a long-term increase in precipitations revealed by the pollen and trace elements data. This is consistent with productivity records which showed a small enhancement in the last 200 years observed from organic carbon flux, TOC (%), and opal reconstruction; furthermore, slight rises in Pb and Fe were observed, suggesting higher continental inputs during this period. This is also consistent with an increase in human activities in the area, particularly intense mining activities and changes in land use that have promoted soil erosion. However, our evidence is still weak to sustain centennial time scale records since our observations are based on few data from surface sediments. This is also less consistent with diatom abundance which was low due to the few records analyzed, in part explaining the inconsistencies between the rise in organic flux and low diatom abundance. Otherwise, this could be explained by the fact that during the El Niño conditions, the normal dominance of diatoms is replaced by smaller size phytoplankton, resulting in a relevant contribution to overall primary production (Iriarte et al., 2000; Rutlland and Montecino, 2002; Escribano et al., 2004). Other observations for northern Chile suggest the intensification of coastal southerly winds as the enhanced solar heat over the land results in the strengthening of upwelling during warmer ENSO periods. Moreover, this results in a net increase in primary production (Vargas et al., 2007). If coming along with Fe inputs to the bay system, this could explain productivity records during present times. In addition, it provides an important clue to the current climate scenario in which our records seem to be matching.

6. Conclusions

Our results suggest that ocean circulation in our study sites seems to impact both places differently, leaving more variable grain compositions and higher TOC contents in the Guanaqueros Bay (core BGGC5) than in the Tongoy Bay (core BTGC8), with the latter increasingly impacted by terrigenous inputs due to the flow of several creeks during major flooding events. Both core records sustain a reduction of organic flux to the bottoms after cal BP ~6500 and into present times. This is probably due to more humid conditions over time, also sustained by ascending ratios of K/Ca, which can be assumed as a result of higher ENSO variability over time. Some Fe concentrations increments at cal BP >6500, around cal BP 3000 – 4000, and in the past 200 years are consistent with increments in primary productivity proxies suggesting their relevance as nutrient element. However, it also point to inputs by eolian and fluvial transport that seem to become relevant after cal BP 6500 to boost phytoplankton during less intense upwelling periods. The last assumption considers that more humid conditions were favored by a less intense SPSA. Thus, the record of continental proxies suggests a long-term increase in precipitation, consistent with previous reconstructions in central Chile. The most distinctive changes were observed after cal BP 6500, when an overall expansion of the coastal vegetation occurred as a result of a progressive increase in precipitation and river runoffs, expanding the grain size of the sediments and the higher concentrations of elements with an important continental source (Al, Fe, K and Pb).

Differences in redox conditions in our records are consistent with less intense upwelling and more frequent oxygenations of the bottoms occurring during the El Niño-like conditions. This could be reconstructed from EFs variations and sensitive redox metal accumulation in the sediments. A clear decreasing trend in Me/Al ratios was apparent, suggesting less oxygen at the bottoms before the beginning of recent times (cal BP ~1700), followed by a rapid change to a more oxygenated environment. Oxygen content in bottom waters was the most relevant factor in sediment metal enrichment above crustal abundance (highest EFs of U, Mo and Re), since the accumulation of organic carbon and estimated sedimentation rates were low in the area. Therefore, organic carbon burial rate is less relevant than oxygen content for the accumulation of metals within the sediments.

Our results suggest that maximum suboxia-anoxia occurred at cal BP ~6500, when peak U, Mo and Re were recorded, probably in a sulfidic environment.

The nutrient-type elements follow a similar trend: lower values at present and higher ratios around cal BP 6500 (Ca, Ni, P and Cd). Their distribution is consistent with diatom and opal distributions, showing their dependence on primary productivity and organic carbon burial rates. If the kinetics reaction is working at low rates for these elements, they should be highly influenced during oxygenation periods, something that seems to have been operating at higher frequencies suggesting more frequent El Niño-like conditions.

Increased regional precipitations have been commonly interpreted by a northward shift of the Southern Westerly Winds belts, yet the higher frequency of El Niño events more likely introduced a high variability of humidity after cal BP 5000. Thus, the apparent rise of oxygen conditions at bottoms could have been the result of this oceanographic feature, which introduced a more oxygenated water mass to the shelf and bays, temporarily changing the redox conditions in surface sediments and affecting the sensitive elements to potential redox changes in the environment. Additionally, this also impacted the accumulation of organic matter due to an intensification of its remineralization, showing a decreasing trend in the buildup of nutrient type elements and organic carbon burial rates towards the present.

Finally, our results suggest that the geochemistry and sedimentary properties of coastal shelf environments in north-central Chile have changed considerably during the Holocene period, suggesting two relevant changes in redox conditions at cal BP 6500, pointing to a change to a less reducing environment which becomes very strong after cal BP 2000. In particular, decreasing trends in primary productivity after cal BP 6500 and increasing trends in oxygenation highlight the sensitivity of these environments to regional climate changes at different timescales. Future changes are therefore likely to be expected in the ongoing scenario of environmental changes at unprecedented rates.

7. References

Abrantes, F.: Diatom assemblages as upwelling indicators in surface sediments off Portugal, Mar. Geol., 85(1), 15–39, doi:10.1016/0025-3227(88)90082-5, 1988.

Ancapichún, S., Garcés-Vargas, J.: Variability of the Southeast Pacific Subtropical Anticyclone and its impact on sea surface temperature off north-central Chile Variabilidad del Anticiclón Subtropical del Pacífico Sudeste y su impacto sobre la temperatura superficial del mar frente a la costa centro-norte de Chile, Cienc. Mar., 41(1), 1–20, DOI:10.7773/cm.v41i1.2338, 2015.

Appleby, P. G. and Oldfield, F.: The calculation of lead-210 dates assuming a constant rate of supply of unsupported210Pb to the sediment, Catena, 5(1), 1–8, doi:10.1016/S0341-8162(78)80002-2, 1978.

Bevington, P. and Robinson, K. (Eds.): Error analysis. In: Data Reduction and Error Analysis for the Physical Sciences, WCB/McGraw-Hill, USA, 38–52, 1992

Blasco, D., Estrada, M. and Jones, B. H.: Short time variability of phytoplankton populations in upwelling regions-the example of Northwest Africa. In: Coastal upwelling. F. A. Richards (Ed.), AGU Washington DC, 339 – 347, 1981

Blott, S. J. and Pye, K.: Gradistat: A Grain Size Distribution and Statistics Package for the Analysis of Unconcolidated Sediments, Earth Surf. Process. Landforms, 26, 1237–1248, doi:10.1002/esp.261, 2001.

Böning, P., Brumsack, H.-J., Schnetger, B., Grunwald, M.: Trace element signatures of Chilean upwelling sediments at 36_S. Mar. Geol., 259, 112–121, 2009.

Calvert, S. E. and Pedersen, T. F.: Geochemistry of Recent oxic and anoxic marine sediments: Implications for the geological record, Mar. Geol., 113(1–2), 67–88, doi:10.1016/0025-3227(93)90150-T, 1993.

Calvert, S. E. and Pedersen, T. F.: Chapter Fourteen Elemental Proxies for Palaeoclimatic and Palaeoceanographic Variability in Marine Sediments: Interpretation and Application, Dev. Mar. Geol., 1(7), 567–644, doi:10.1016/S1572-5480(07)01019-6, 2007.

Carré, M., Sachs, J.P., Purca, S., Schauer, A.J., Braconnot, P., Falcón, R.A., Julien, M., Lavallée, D.: Holocene history of ENSO variance and asymmetry in the eastern tropical Pacific, Science 345, 1045–1048. 2014. DOI: 10.1126/science.1255768

Carré, M., Jackson, D., Maldonado, A., Chase, B.M., Sachs, J.P.: Variability of 14C reservoir age and air–sea flux of CO2 in the Peru–Chile upwelling region during the past 12,000 years, Quat. Res., 85, 87–93, 2016.

Chaillou, G., Anschutz, P., Lavaux, G., Schäfer, J. and Blanc, G.: The distribution of Mo, U, and Cd in relation to major redox species in muddy sediments of the Bay of Biscay, Mar. Chem., 80(1), 41–59, doi:10.1016/S0304-4203(02)00097-X, 2002.

Colodner, D., Sachs, J., Ravizza, G., Turekian, K. K. and Boyle, E.: The geochemical cycle of Re: a reconnaissance, Earth Planet. Sci. Lett., 117, 205–221, doi:10.1016/0012-821X(93)90127-U, 1993.

Croquette, M., Eldin, G., Grados, C., Tamayo, M.: 2007. On differences in satellite winds product and their effects in estimating coastal upwelling processes in the South-east Pacific, Geophys. Res. Lett., 34 L11 608, doi: 10.1029/2006GL027538.

Crusius, J., Calvert, S., Pedersen, T. and Sage, D.: Rhenium and molybdenum enrichments in sediments as indicators of oxic, suboxic and sulfidic conditions of deposition, Earth Planet. Sci. Lett., 145(1–4), 65–78, doi:10.1016/S0012-821X(96)00204-X, 1996.

Daneri, G., Dellarossa, V., Quiñones, R., Jacob, B., Montero, P. and Ulloa, O.: Primary production and community respiration in the Humboldt Current System off Chile and associated oceanic areas, Mar. Ecol. Prog. Ser., 197, 41–49, doi:10.3354/meps197041, 2000.

Dearing, J., Magnetic susceptibility. In: Environmental Magnetism: A Practical Guide. Walden, J., Oldfield, F., and Smith, J. (Eds.), Quaternary Research Association Technical Guide No. 6, London, 35–62, 1999.

De Pol-Holz, R., Ulloa, O., Lamy, F., Dezileau, L., Sabatier, P., and Hebbeln, D.: Late Quaternary variability of sedimentary nitrogen isotopes in the eastern South Pacific Ocean, Paleoceanography, 22, PA2207, doi: 10.1029/2006 PA001308, 2007.

Dezileau, L., Ulloa, O., Hebbeln, D., Lamy, F., Reyss, J. L. and Fontugne, M.: Iron control of past productivity in the coastal upwelling system off the Atacama Desert, Chile, Paleoceanography, 19(3), doi:10.1029/2004PA001006, 2004.

Dymond, J., Suess, E. and Lyle, M.: Barium in deep-sea sediment: A geochemical proxy for paleoproductivity, Paleoceanography, 7(2), 163–181, 1992.

Escribano, R., Daneri, G., Farías, L., Gallardo, V. A., González, H. E., Gutiérrez, D., Lange, C. B., Morales, C. E., Pizarro, O., Ulloa, O. and Braun, M.: Biological and chemical consequences of the 1997-1998 El Niño in the Chilean coastal upwelling system: A synthesis, Deep. Res. Part II Top. Stud. Oceanogr., 51(20–21), 2389–2411, doi:10.1016/j.dsr2.2004.08.011, 2004.

Faegri, K. and Iversen, J.: Textbook of pollen analysis, IV. The Blackburn Press, New Yersey, 328 pp., 1989.

Figueroa, D. and Moffat, D.: On the influence of topography in the induction of coastal upwelling along the Chilean coast Geophys. Res. Lett. 27, 3905-3908, 2000.

Flynn, W. W.: The determination of low levels of polonium-210 in environmental materials, Anal. Chim. Acta, 43, 221–227, 1968.

Gallardo, M.A., González, A., Ramos, M., Mujica, A., Muñoz, P., Sellanes, J., Yannicelli, B.: Reproductive patterns in demersal crustaceans from the upper boundary of the OMZ off north-central Chile, Cont. Shelf. Res. 141, 26–37, 2017.

Ganeshram, R.S., Pedersen, T. F., Calvert, S.G.,McNeill, G., Fontugne, M.: Glacial-interglacial variability in denitrification in the world's oceans: Causes and consequences. Paleoceanography, 15(4), 361– 376, 2000.

Garreaud, R. and Rutllant, J.: Análisis meteorológico de los aluviones de Antofagasta y Santiago de Chile en el período 1991–1993, Atmósfera, 9, 251–271, 1996.

Garreaud, R., Barichivich, J., Christie, D., Maldonado, A.: Interanual variability of the coastal fog at Fray Jorge relict forest in semiarid Chile. Journal of Geophysical Research. Vol 113. G04011, 2008. doi:10.1029/2008JG000709.

Garreaud, R., Vuille. M., Compagnuccic, R. and Marengo, J.: Present-day South American climate, Palaeogeogr. Palaeocl., 281, 180-195, 2009 doi:10.1016/j.palaeo.2007.10.032

Govin, A., Holzwarth, U., Heslop, D., Ford Keeling, L., Zabel, M., Mulitza, S., Collins, J. A. and Chiessi, C. M.: Distribution of major elements in Atlantic surface sediments (36°N-49°S): Imprint of terrigenous input and continental weathering, Geochemistry, Geophys. Geosystems, 13(1), 1–23, doi:10.1029/2011GC003785, 2012.

Gutiérrez, D., Sifedine, A., Reyss, J.L., Vargas, G., Velazco, F., Salvattci, R., Ferreira, V., Ortlieb, L., Field, D., Baumgartner, T., Boussafir, M., Boucher, H., Valdés, J., Marinovic, L., Soler, P., Tapia, P: Anoxic sediments off Central Peru record interannual to multidecadal changes of climate and upwelling ecosystem during the last two centuries, Adv. Geosci. 6, 119–125, 2006.

Gutiérrez, D., Enríquez, E., Purca, S., Quipuzcoa, L., Marquina, R., Flores, G. and Graco, M.: Oxygenation episodes on the continental shelf of central Peru: Remote forcing and benthic ecosystem response. Prog. Oceanogr., 79, 177–189, 2008.

Hansen, H. P., Koroleff, F.: Determination of nutrients. In Methods of Seawater Analysis. Grasshoff, K., Kremling, K. and Ehrhardt, M. (Eds.), Wiley-VCH Verlag GmbH, Weinheim, Germany, 159–228, 1999.

Hatfield, R. G., Stoner, J. S.: Magnetic Proxies and Susceptibility. In: The Encyclopedia of Quaternary Science. Elias, S.A. (ed.) 2, 884-898, 2013.

Hebbeln, D., Marchant, M., Freudenthal, T., Wefer, G.: Surface distribution along the Chilean continental slope related to upwelling and productivity. Marine Geology 164, 119–137, 2000.

Hebbeln, D., Marchant, M. and Wefer, G.: Paleoproductivity in the southern Peru ^ Chile Current through the last 33 000 yr, Mar. Geol., 186, 2002.

Helly, J. and Levin. L.: Global distribution of naturally occurring marine hypoxia on continental margin, Deep-Sea Res. Pt. I, 51, 1159-1168, 2004.

Heusser, C. J. and Moar, N. T.: Pollen and spores of chile: Modern types of the pteridophyta, gymnospermae, and angiospermae, New Zeal. J. Bot., 11(2), 389–391, doi:10.1080/0028825X.1973.10430287, 1973.

Huerta-Diaz, M. A. and Morse, J. W.: Pyritization of trace metals in anoxic marine sediments, Geochim. Cosmochim. Acta, 56(7), 2681–2702, doi:10.1016/0016-7037(92)90353-K, 1992.

Iriarte, J.L. and González, H.: Phytoplankton size structure during and after the 1997/98 El Niño in a coastal upwelling area of the northern Humboldt Current System, Mar. Ecol. Prog. Ser., 269, 83 – 90, 2004.

Jenny, B., Wilhelm, D., Valero-Garcés, B.L.: The Southern Westerlies in Central Chile: Holocene precipitation estimates based on a water balance model for Laguna Aculeo (33°50’S), Clim. Dynam., 20, 269–280, DOI 10.1007/s00382-002-0267-3, 2003.

Kaiser, J., Schefuß, E., Lamy, F., Mohtadi, M., Hebbeln, D.:Glacial to Holocene changes in sea surface temperature and coastal vegetation in north central Chile: high versus low latitude forcing, Quat. Sci. Rev., 27, 2064–2075, 2008.

Keshav, N. and Achyuthan, H.: Late Holocene continental shelf sediments, off Cuddalore, East coast, Bay of Bengal, India: Geochemical implications for source-area weathering and provenance, Quat. Int., 371, 209–218, doi:10.1016/j.quaint.2015.03.002, 2015.

Klinkhammer, G. P. and Palmer, M. R. Uranium in the oceans: Where it goes and why, Geochim. Cosmochim. Ac., 55(7), 1799–1806, doi: 10.1016/0016-037(91)90024-Y, 1991.

Koutavas, A. and Joanides, S.: El Niño–Southern Oscillation extrema in the Holocene and Last Glacial Maximum, Paleoceanography, 27, PA4208, 2012. doi:10.1029/2012PA002378.

Koutavas, A., deMenocal, P.B., Olive, G.C., Lynch-Stieglitz, J.: Mid-Holocene El Niño–Southern Oscillation (ENSO) attenuation revealed by individual foraminifera in eastern tropical Pacific sediments, 34(12), 993–996, doi: 10.1130/G22810A, 2006.

Lambeck, K., Rouby, H., Purcella, A., Sunc, Y., Sambridge, M.: Sea level and global ice volumes from the Last Glacial Maximum to the Holocene, PNAS, 111(43), 15296-15303, 2014.

Lamy F., Hebbeln, D., Wefer, G.: High-Resolution Marine Record of Climatic Change in Mid-latitude Chile during the Last 28,000 Years Based on Terrigenous Sediment Parameters, Quat. Res., 51**,** 83–93, 1999.

Lamy, F., Kilian, R., Arz, H.W., Francois J-P., Kaiser, J.,Prange, M. and Steinke, T.: Holocene changes in the position and intensity of the southern westerly wind belt, Nat. Geosci., 3, 695–699, 2010.

Little, S. H., Vance, D., Walker-Brown, C. and Landing, W. M.: The oceanic mass balance of copper and zinc isotopes, investigated by analysis of their inputs, and outputs to ferromanganese oxide sediments, Geochim. Cosmochim. Acta, 125, 673–693, doi:10.1016/j.gca.2013.07.046, 2014.

Maldonado, A., Villagrán, C.,:Paleoenvironmental changes in the semiarid coast of Chile (~32°S) during the last 6200 cal years inferred from a swamp-forest pollen record. Quat. Res., 58, 130–138, 2002.

Maldonado, A. and Rozas, E.: Clima y Paleoambientes durante el Cuaternario Tardío en la Región de Atacama, in Libro Rojo de la Flora Nativa y de los Sitios Prioritarios para su Conservación: Región de Atacama, pp. 293–304., 2008.

Maldonado, A. and Villagrán, C.: Climate variability over the last 9900 cal yr BP from a swamp forest pollen record along the semiarid coast of Chile, Quat. Res., 66(2), 246–258, doi:10.1016/j.yqres.2006.04.003, 2006.

Maldonado, A., ME. de Porras, A. Zamora & AM. Abarzúa. El escenario geográfico y paleoambiental de Chile. Capitulo I. Culturas de Chile. Prehistoria. Desde sus orígenes hasta los albores de la conquista. F. Falabella & M. Uribe. Eds. Editorial Andrés Bello. 2016.

Mazzullo, J., Gilbert, A., Rabinowitz, P., Meyer, A. and Garrison, L.: Handbook for Shipboard Sedimentologists, 67 pp., 1988.

McManus, J., Berelson, W. M., Severmann, S., Poulson, R. L., Hammond, D. E., Klinkhammer, G. P., and Holm, C.: Molybdenum and uranium geochemistry in continental margin sediments: Paleoproxy potential, Geochim. Cosmochim. Acta, 70, 4643–4662, 2006.

Merino-Campos, V., De Pol-Holz, R. Southon, J., Latorre, C., Collado-Fabbri, S.: Marine radiocarbon reservoir age along the Chilean continental margin, Radiocarbon, 81, 1–16, doi:10.1017/RDC.2018.81, 2018.

Montecinos, A., and Aceituno, P.: Seasonality of the ENSO-Related Rainfall Variability in Central Chile and Associated Circulation Anomalies. J. Climate., 16, 281–296, 2003.

Montecinos, S., Gutiérrez, J. R., López-Cortés, F. and López, D.: Climatic characteristics of the semi-arid Coquimbo Region in Chile, J. Arid Environ., 126, 7–11, doi:10.1016/j.jaridenv.2015.09.018, 2016.

Moraga-Opazo, J., Valle-Levinson, A., Ramos, M. and Pizarro-Koch, M.: Upwelling-Triggered near-geostrophic recirculation in an equatorward facing embayment, Cont. Shelf Res., 31, 1991–1999, 2011.

Mortlock, R. A. and Froelich, P. N.: A simple method for the rapid determination of biogenic opal in pelagic marine sediments, Deep Sea Res. Part A, Oceanogr. Res. Pap., 36(9), 1415–1426, doi:10.1016/0198-0149(89)90092-7, 1989.

Morse, J.W. and Luther, G.W.: Chemical influences on trace metal–sulfide interactions in anoxic sediments. Geochim Cosmochim Ac., 63, 3373–3378, 1999.

Nakanishi, T. and Minagawa, M.: Stable carbon and nitrogen isotopic compositions of sinking particles in the northeast Japan Sea, Geochem. J., 37(2), 261–275, doi:https://doi.org/10.2343/geochemj.37.261, 2003.

Nameroff, T., Balistrieri, L. and Murray, W.: Suboxic trace metals geochemistry in the eastern tropical North Pacific, Geochim Cosmochim Ac., 66(7), 1139–1158, 2002.

Ogrinc, N., Fontolan, G., Faganeli, J. and Covelli, S.: Carbon and nitrogen isotope compositions of organic matter in coastal marine sediments (the Gulf of Trieste, N Adriatic Sea): indicators of sources and preservation, Mar. Chem., 95, 163-181, 2005.

Ohnemus, D. C. and Lam, P. J.: Cycling of lithogenic marine particles in the US GEOTRACES North Atlantic transect, Deep. Res. Part II Top. Stud. Oceanogr., 116, 283–302, doi:10.1016/j.dsr2.2014.11.019, 2015.

Ortega, C., Vargas, G., Rutllant, J.A., Jackson, D., Méndez, C.: Major hydrological regime change along the semiarid western coast of South America during the early Holocene, Quaternary Res., 78, 513-527, 2012.

Ortega, C., Vargas, G., Rojas, M., Rutllant, J.A., Muñoz, P., Lange, C.B., Pantoja, S., Dezileau, L., Ortlieb, L.: Extreme ENSO-driven torrential rainfalls at the southern edge of the Atacama Desert during the late Holocene and their projection into the 21th century, GloPlaCha, 175, 226–237, 2019. https://doi.org/ 10.1016/j.gloplacha.2019.02.011

Paytan, A.: Ocean paleoproductivity, Encyclopedia of Paleoclimatology and Ancient Environments, Encyclopedia of Earth Science Series, Gornitz, V. (Ed.), Kluwer Academic Publishers. 2008.

Peacock, C.L. and Sherman, D.M.: Copper(II) sorption onto goethite, hematite and lepidocrocite: a surface complexation model based on ab initio molecular geometries and EXAFS spectroscopy. Geochim. Cosmochim. Ac., 68, 2623–2637, 2004.

Pizarro, O., Hormazabal, S., Gonzalez, A. and Yañez, E.: Variabilidad del viento, nivel del mar y temperatura en la costa norte de Chile, Invest. Mar., 22, 85–101, 1994.

Pizarro, O., Shaffer, G., Dewitte, B. and Ramos, M.: Dynamics of seasonal and interannual variability of the Peru-Chile Undercurrent, Geophys. Res. Lett., 29(12), 28–31, doi:10.1029/2002GL014790, 2002.

Quintana, J.M. and Aceituno, P.: Changes in the rainfall regime along the extratropical west coast of South America (Chile): 30-43º S, Atmosfera, 25(1), 1 – 22, 2012.

Ramos, M., Pizarro,O., Bravo, L. and Dewitte, B.: Seasonal variability of the permanent thermocline off northern Chile, Geophys. Res. Lett., 33, L09608, doi:10.1029/2006GL025882, 2006.

Ramos, M., Dewitte, B., Pizarro, O. and Garric, G.: Vertical propagation of extratropical Rossby waves during the 1997–1998 El Niño off the west coast of South America in a medium-resolution OGCM simulation, J. Geophys. Res., 113, C08041, doi:10.1029/2007JC004681, 2008.

Rau, H. G., Takahashi, T. and Des Marais, D. J.: Latitudinal variations in plankton δ13C: implications for CO2 and productivity in past oceans, Nature, 341, 516–518, 1989.

Rahn, D.A. and Garreaud, R.A.: A synoptic climatology of the near-surface wind along the west coast of South America. Int. J. Climatol., 2013. DOI: 10.1002/joc.3724.

Reimer, P. J., Bard, E., Bayliss, A., Beck, J. W., Blackwell, P. G., Ramsey, C. B., Buck, C. E., Cheng, H., Edwards, R. L., Friedrich, M., Grootes, P. M., Guilderson, T. P., Haflidason, H., Hajdas, I., Hatté, C., Heaton, T. J., Hoffmann, D. L., Hogg, A. G., Hughen, K. A., Kaiser, K. F., Kromer, B., Manning, S. W., Niu, M., Reimer, R. W., Richards, D. A., Scott, E. M., Southon, J. R., Staff, R. A., Turney, C. S. M. and van der Plicht, J.: IntCal13 and Marine13 Radiocarbon Age Calibration Curves 0–50,000 Years cal BP, Radiocarbon, 55(4), 1869–1887, doi:10.2458/azu_js_rc.55.16947, 2013.

Rein, B., Lückge, A., Reinhardt, L., Sirocko, F., Wolf, A., Dullo, W-C.: El Niño variability off Peru during the last 20,000 years, Paleoceanogr., PA4003, doi:10.1029/2004PA001099, 2005

Rutlland, J. and Fuenzalida, H.: Synoptic aspects of the central Chile Rainfall variability associated with the southern oscillation, Int. J. Climatol., 11, 63 − 76, 1991.

Rutlland, J. and Montecino, V.: Multiscale upwelling forcing cycles and biological response off northcentral Chile, Rev. Chil. Hist. Nat., 7, 217-231, 2002

Sabatier, P., Dezileau, L., Blanchemanche, P., Siani, G., Condomines, M., Bentaleb, I. and Piquès, G.: Holocene variations of radiocarbon reservoir ages in a mediterranean lagoonal system, Radiocarbon, 52(1), 91–102, doi:10.1017/S0033822200045057, 2010.

Saito, C., Noriki, S. and Tsunogai, S.: Particulate flux of Ai, a component of land origin, in the western North Pacific, Deep-Sea Res., 39, 1315–1327, 1992.

Salvatteci, R., Gutiérrez, D., Field, D., Sifeddine, A., Ortlieb, L., Bouloubassi, I., Boussafir, M., Boucher, H. and Cetin, F.: The response of the Peruvian Upwelling Ecosystem to centennial-scale global change during the last two millennia, Clim. Past, 10(2), 715–731, doi:10.5194/cp-10-715-2014, 2014.

Schrader H. J. and Gersonde, R.: Diatoms and silicoflagellates. Utrecht Micropaleontol. Bull. 17, 129–176, 1978.

Sellanes, J., Quiroga, E., Neira, C., Gutiérrez, D.: Changes of macrobenthos composition under different ENSO cycle conditions on the continental shelf off central Chile, Cont. Shelf. Res. 27, 1002 −1016, 2007.

Siebert, C., Nägler, T.F., von Blackenburg, F., Kramers, J.D.: Molybdenum isotope records as a potential new proxy for paleoceanography. Earth Planet. Sci. Lett., 6643, 1–13, 2003.

Shaffer, G., Pizarro, O. Djurfeldt, L., Salinas, S. and Rutllant, J.: Circulation and low-frequency variability near the Chilean coast: Remotely forced fluctuations during the 1991– 92 El Niño, J. Phys. Oceanogr., 27, 217– 235, 1997.

Sigman, D.M., Karsh, K.L., Casciotti, K.L.: Ocean process tracers: nitrogen isotopes in the ocean. Encyclopedia of ocean science, 2nd edn Elsevier, Amsterdam.
Sims, P.A. 1996. An Atlas of British Diatoms. Biopress Ltd, Bristol United Kingdom 601, 2009.

Sun, X., Higgins, J. and Turchyn, A. V.: Diffusive cation fluxes in deep-sea sediments and insight into the global geochemical cycles of calcium, magnesium, sodium and potassium, Mar. Geol., 373, 64–77, doi:10.1016/j.margeo.2015.12.011, 2016.

Sundby, B., Martinez, P. and Gobeil, C.: Comparative geochemistry of cadmium, rhenium, uranium, and molybdenum in continental margin sediments, Geochim. Cosmochim. Ac., 68, 2485–2493, 2004.

Sweeney, R. E., Kaplan I. R.: Natural abundances of 15N as a source indicator of nearshore marine sedimentary and dissolved nitrogen, Mar. Chem., 9, 81− 94, 1980.

Thiel, M., Macaya, E.C., Acuña, E., Artnz, W.F., Bastias. H., Brokordt. K., Camus, P.A., Castilla, J.C., Castro, L.R., Cortés, M., Dumont, C.P., Escribano, R., Fernandez, M., Gajardo, J.A., Gaymer, C.F., Gómez, I., González, A.E., González, H.E., Haye, P., Illanes, J.E., Iriarte, J.L., Lancellotti, D.A., Luna-Jorquera, G., Luxoro, C., Manriquez, P.H., Marín, V., Muñoz, P., Navarrete, S.A., Pérez, E., Poulin, E., Sellanes, J., Sepúlveda, H.H., Stotz, W., Tala, F., Thomas, A., Vargas, C.A., Vásquez, J.A., Vega, J.M.: The Humboldt Current system of Northern and Central Chile: Oceanographic processes, ecological interactions and socioeconomic feedback. Oceanogr. Mar. Biol. An Annual Review, 45, 195‒344, 2007.

Torres, M. E., Brumsack, H. J., Bohrman, G. and Emeis, K. C.: Barite front in continental margin sediments: a new look at barium remobilization in the zone of sulfate reduction and formation of heavy barites in diagenetic fronts, Chem. Geol., 127, 125–139, 1996.

Torres, R., and Ampuero, P.: Strong CO2 outgassing from high nutrient low chlorophyll coastal waters off central Chile (30°S): The role of dissolved iron, Estuar. Coast. Shelf S., 83, 126‒132, doi:10.1016/j.ecss.2009.02.030, 2009.

Tribovillard, N., Algeo, T. J., Lyons, T. and Riboulleau, A.: Trace metals as paleoredox and paleoproductivity proxies: an update. Chem. Geol., 232, 12–32, 2006.

Vance, D., Archer, C., Bermin, J., Perkins, J., Statham, P. J., Lohan, M. C., Ellwood, M. J. and Mills, R. A.: The copper isotope geochemistry of rivers and the oceans, Earth Planet. Sc. Lett., 274, 204–213, 2008.

Valle-Levinson, A., Moraga, J., Olivares, J. and Blanco, J. L.: Tidal and residual circulation in a semi-arid bay: Coquimbo Bay, Chile. Cont. Shelf Res., 20, 2009–2018, 2000.

Valle-Levinson, A. and Moraga-Opazo, J.: Observations of bipolar residual circulation in two equatorward-facing semiarid bays, Cont. Shelf Res., 26(2), 179–193, doi:10.1016/j.csr.2005.10.002, 2006.

Van der Weijden, C.: Pitfalls of normalization of marine geochemical data using a common divisor, Mar. Geol., 184, 167–187, 2002.

Vargas, G., Ortlieb, L., Pichon, J. J., Bertaux, J. and Pujos, M.: Sedimentary facies and high resolution primary production inferences from laminated diatomacous sediments off northern Chile (23°S), Mar. Geol., 211(1–2), 79–99, doi:10.1016/j.margeo.2004.05.032, 2004.

Vargas, G., Rutllant, J., Ortlieb, L.: ENSO tropical–extratropical climate teleconnections and mechanisms for Holocene debris flows along the hyperarid coast of western South America (17°–24°S), Earth Planet. Sci. Lett., 249, 467–483, 2006.

Vargas, G., Pantoja, S., Rutllant, J., Lange, C. and Ortlieb, L.: Enhancement of coastal upwelling and interdecadal ENSO-like variability in the Peru-Chile Current since late 19th century. Geophys. Res. Lett., 34, L13607, 2007.

Ulloa, O., Escribano, R., Hormazabal, S., Quiñones, R.A., Gonzalez, R., Ramos, M.,: Evolution and biological effects of the 1997-98 E1 Niño in the upwelling ecosystem off northern Chile, Geophys. Res. Lett., 28, 1591– 1594, 2001.

Ulloa, O., Canfield, D.E., DeLong, E.F., Letelier, R.L. and Stewart, F.J.: Microbial oceanography of anoxic oxygen minimum zones. PNAS, 109, 15996–16003, 2012. doi/10.1073/pnas.1205009109

Veit, H.: Southern Westerlies during the Holocene deduced from geomorphological and pedological studies in the Norte Chico, Northern Chile (27–33°S). *Palaeogeogr., Palaeoclimatol., Palaeoecol.,* 123**,** 107–119, 1996.

Williams, P. M. and Gordon, L. I.: Carbon-13:carbon-12 ratios in dissolved and particulate organic matter in the sea. Deep-Sea Res., 17, 19–27, 1970.

Xu, G., Liu, J., Pei, S., Kong, X., Hu, G. and Gao, M.: Source identification of aluminum in surface sediments of the Yellow Sea off the Shandong Peninsula, Acta Oceanol. Sin., 34(12), 147–153, doi:10.1007/s13131-015-0766-9, 2015.

Zheng, Y., Anderson, R. F., van Geen, A. and Fleisheir, M.Q.: Preservation of non-lithogenic particulate uranium in marine sediments. Geochim. Cosmochim. Ac., 66, 3085–3092, 2002.

Acknowledgments

We would like to thank the R/V Stella Maris II crew of Universidad Católica del Norte for their help and support during field work. We extend our acknowledgements to the laboratory assistants of the Paleoceanography Lab at Universidad de Concepción, for their aid in sample analyses. We also wish to thank Dr. Olivier Bruguier of CNRS and his lab personnel for their assistance during ICPMs analyses. We also express our gratitude to INNOVA 07CN13 IXM-150, FONDECYT 1180413 and FONDECYT 1170408. This manuscript was mainly funded by FONDECYT Project No. 1140851. Partial support from the COPAS Sur-Austral (CONICYT PIA PFB31) and FONDAP-IDEAL centers (No. 15150003) is also acknowledged.

Tables

Table 1. Radiocarbon dates for BGGC5 and BTGC8 sediment cores collected from mixed planktonic foraminifera and monospecific benthic foraminifera (*Bolivina plicata*), respectively. The ^{14}C-AMS was performed at NOSAM-WHOI. The lab code and conventional ages collected from each core section is indicated. For error calculations see http://www.whoi.edu/nosams/radiocarbon-data-calculations.

Core identification	Material	Mass (mg)	Lab Code NOSAM	Modern fraction pMC	1σ error	Conventional Age BP	1σ error
BGGC5	Planktonic foraminifera						
10-11	mix	1.8	OS-122160	0.8895	0.0027	940	25
18-19	mix	1.1	OS-122141	0.7217	0.0024	2,620	25
31-32	mix	2.7	OS-122161	0.6590	0.0021	3,350	25
45-46	mix	2.0	OS-122162	0.6102	0.0017	3,970	25
55-56	mix	1.6	OS-122138	0.5864	0.0025	4,290	35
66-67	mix	2.8	OS-122304	0.5597	0.0018	4,660	25
76-77	mix	2.6	OS-122163	0.4520	0.0016	6,380	30
96-97	mix	1.1	OS-122139	0.4333	0.0033	6,720	60
115-116	mix	4.7	OS-122164	0.3843	0.0016	7,680	35
BTGC8	Benthic foraminifera						
5-6	Bolivina plicata	4.2	OS-130657	0.8953	0.0017	890	15
20-21	Bolivina plicata	7.7	OS-123670	0.7337	0.0021	2,490	25
30-31	Bolivina plicata	13.0	OS-123671	0.6771	0.0016	3,130	20
40-41	Bolivina plicata	11.0	OS-123672	0.6507	0.0019	3,450	25
50-51	Bolivina plicata	8.7	OS-123673	0.5877	0.0014	4,270	20
60-61	Bolivina plicata	13.0	OS-123674	0.5560	0.0018	4,720	25
71-72	Bolivina plicata	10.0	OS-123675	0.4930	0.0013	5,680	20
80-81	Bolivina plicata	7.3	OS-123676	0.4542	0.0012	6,340	20
90-91	Bolivina plicata	6.8	OS-123677	0.4259	0.0015	6,860	30
96-97	Bolivina plicata	6.8	OS-123678	0.3903	0.0013	7,560	25

Table 2. Reservoir age (DR) estimation considering the ^{210}Pb age determined with the CRS model (McCaffrey and Thomson, 1980) at a selected depth sections of the core, compared with ^{14}C ages (yr BP) from marine13.14 curve (Reimer et al., 2013), according to Sabatier et al. (2010).

Core	Depth (cm)	Age from CRS model (AD)[a]	Age years BP[b]	^{14}C age Marine 13.14	^{14}C age BP from foram.	DR
BGGC5	10.5	1828	122	499±24	940±25	441±35
BTCG8	5.5	1908	42	448±23	890±15	442±27

[a]Anno Domini
[b]Before present=1950

Table 3. Concentration of elements in Pachingo wetland sediments, considered as lithogenic background for the study area. The values correspond to mean concentrations in surface sediments (0−3 cm).

Element	Metal/Al x 10^3	s
Ca	686.5	139.3
Fe	591.3	84.5
P	8.6	0.7
Sr	5.7	0.6
Ba	5.6	0.1
Cu	0.258	0.019
Ni	0.174	0.005
U	0.020	0.003
Mo	0.020	0.003
Cd	0.0021	0.0003
Re	0.00004	0.00001

Table 4. Mean authigenic enrichment factor (EF) ± SD of trace elements calculated for Guanaqueros Bay (BGGC5 core). Lithogenic background was estimated from surface sediments of Pachingo wetland cores (see text). Age ranges were based on the variability of diatoms abundance (valves g^{-1}).

Age range (cal BP)	**Diatoms ($x10^6$) (min-max)**	**Opal ($g\ m^{-2}\ yr^{-1}$) (min-max)**	**EF_U**	**EF_{Mo}**	**EF_{Re}**	**EF_{Fe}**	**EF_{Ba}**	**EF_{Cd}**	**EF_{Ni}**	**EF_{Cu}**	**EF_P**
-65 – 130	0.5 – 4.9	3 − 40	2.6 ±0.7	5.5 ±1.3	10.5 ±2.0	0.8 ±0.1	0.8 ±0.1	30.3 ±6.3	1.4 ±0.2	3.6[a] ±1.3	2.0 ±0.4
130 − 1700	0.6 – 1.7	1 − 3	5.6 ±1.4	14.5 ±3.7	18.4 ±3.8	0.9 ±0.1	0.8 ±0.1	40.6 ±3.7	1.9 ±0.1	3.0 ±0.4	2.4 ±0.4
1700 − 4500	1.9 – 5.4	2 − 21	5.5 ±0.6	14.5 ±1.5	19.8 ±2.0	0.9 ±0.1	0.8 ±0.1	55.1 ±12.2	2.3 ±0.3	3.1 ±0.5	2.2 ±0.3
4500 − 6500	2.7 – 4.5	4 − 47	5.1 ±0.8	16.9 ±3.3	19.5 ±3.0	0.9 ±0.1	0.9 ±0.1	140.1 ±46.3	3.4 ±0.5	3.1 ±0.5	3.2 ±0.5
6500 − 8400	15.7 −41.0	9 − 53	4.5 ±0.4	13.9 ±2.6	17.9 ±2.2	0.9 ±0.1	0.9 ±0.1	142.5 ±24.2	3.4 ±0.4	2.5 ±0.3	3.9 ±0.8

[a]Mean EF_{Cu} after AD 1936 was 4.6 ±0.5

Table 5. Spearman rank order correlations for geochemical data. Significant values >0.8 are indicated in bold.

BGGC5

	Al	**P**	**K**	**Ca**	Mn	**Fe**	**Ni**	**Cu**	**Mo**	**Cd**	**Re**	**Sr**	**U**	**Ba**	**Opal**	**TOC**
Al	1.00	-0.62	0.49	-0.48	0.64	0.60	-0.75	0.56	-0.10	-0.73	-0.08	-0.33	0.08	0.49	-0.52	-0.44
P		1.00	-0.31	0.37	-0.45	-0.56	0.56	-0.57	0.01	0.61	-0.11	0.39	-0.12	-0.20	0.49	0.24
K			1.00	-0.24	**0.90**	**0.83**	-0.29	0.47	0.28	-0.42	0.33	-0.12	0.50	0.26	-0.25	-0.19
Ca				1.00	-0.47	-0.50	0.44	-0.64	0.23	0.59	0.39	**0.92**	0.30	-0.60	0.18	0.32
Mn					1.00	**0.94**	-0.51	0.68	-0.01	-0.68	0.07	-0.32	0.24	0.43	-0.39	-0.31
Fe						1.00	-0.49	**0.81**	0.03	-0.70	0.11	-0.40	0.23	0.36	-0.37	-0.21
Ni							1.00	-0.51	0.49	**0.91**	0.35	0.25	0.26	-0.70	0.72	0.64
Cu								1.00	-0.12	-0.71	-0.06	-0.61	0.00	0.31	-0.39	-0.07
Mo									1.00	0.50	**0.88**	0.10	0.91	-0.48	0.33	0.36
Cd										1.00	0.36	0.42	0.27	-0.67	0.70	0.54
Re											1.00	0.27	**0.92**	-0.50	0.16	0.38
Sr												1.00	0.24	-0.36	0.05	0.17
U													1.00	-0.39	0.10	0.29
Ba														1.00	-0.30	-0.59
Opal															1.00	0.35
TOC																1.00

BTGC8

	Al	**P**	**K**	**Ca**	**Mn**	**Fe**	**Ni**	**Cu**	**Mo**	**Cd**	**Re**	**Sr**	**U**	**Ba**	**Opal**	**TOC**
Al	1.00	-0.19	-0.17	-0.37	-0.02	-0.03	-0.39	-0.04	-0.39	0.02	-0.13	-0.58	-0.19	0.07	-0.41	-0.29
P		1.00	0.23	0.00	0.43	0.28	0.58	0.23	0.37	0.13	-0.04	0.30	0.14	-0.14	0.56	0.13
K			1.00	-0.02	0.54	0.41	0.43	0.22	-0.11	0.05	-0.04	0.19	-0.28	0.28	0.26	0.20
Ca				1.00	-0.33	-0.27	0.00	-0.23	0.39	0.01	0.33	0.50	0.47	-0.34	0.20	0.34
Mn					1.00	0.21	0.64	0.01	0.05	0.33	0.15	0.32	-0.02	0.24	0.32	0.00
Fe						1.00	0.13	0.71	-0.40	-0.48	-0.67	-0.37	-0.62	0.13	0.14	0.10
Ni							1.00	0.24	0.56	0.20	0.25	0.64	0.19	-0.16	**0.80**	0.45
Cu								1.00	-0.25	-0.68	-0.56	-0.22	-0.61	-0.10	0.21	0.37
Mo									1.00	0.45	0.59	0.66	0.69	-0.41	0.58	0.30
Cd										1.00	0.56	0.39	0.52	0.11	0.10	-0.12
Re											1.00	0.53	**0.83**	-0.16	0.13	0.17
Sr												1.00	0.58	-0.13	0.52	0.23
U													1.00	-0.19	0.21	0.00
Ba														1.00	-0.28	-0.42
Opal															1.00	0.39
TOC																1.00

Figures

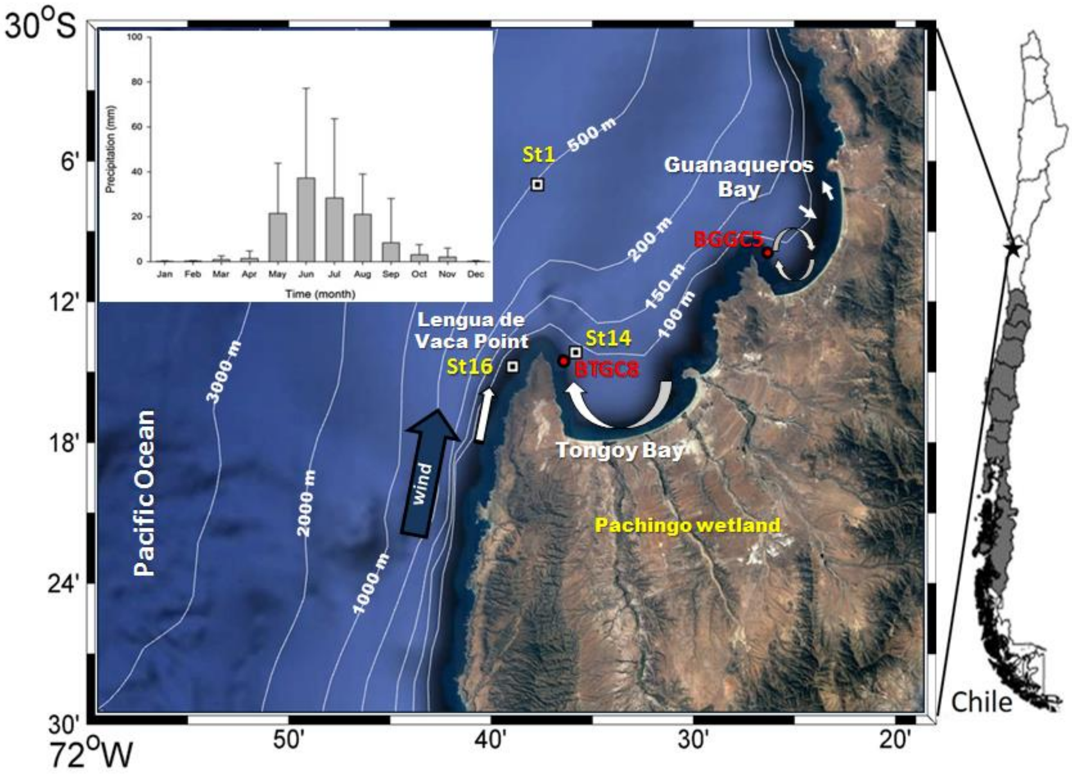

Figure 1. Study area showing the position of sampling stations. Sediment cores were retrieved from Guanaqueros Bay (BGGC5) and from Tongoy Bay (BTGC8) at water depths of 89 and 85 m, respectively. Information of dissolved oxygen (DO) in the water column at ST1and ST16 and of suspended organic particles collected at ST14 sampling sites was gathered in a previous project (INNOVA 07CN13 IXM-150). Monthly precipitation in mm (bars) (means ± SD; Montecinos et al., 2016). Schematic representation of the bays circulation (white arrows) and wind direction is indicated (blue arrow) obtained from Valle-Levinson and Moraga-Opazo (2006) and Moraga-Opazo et al. (2011).

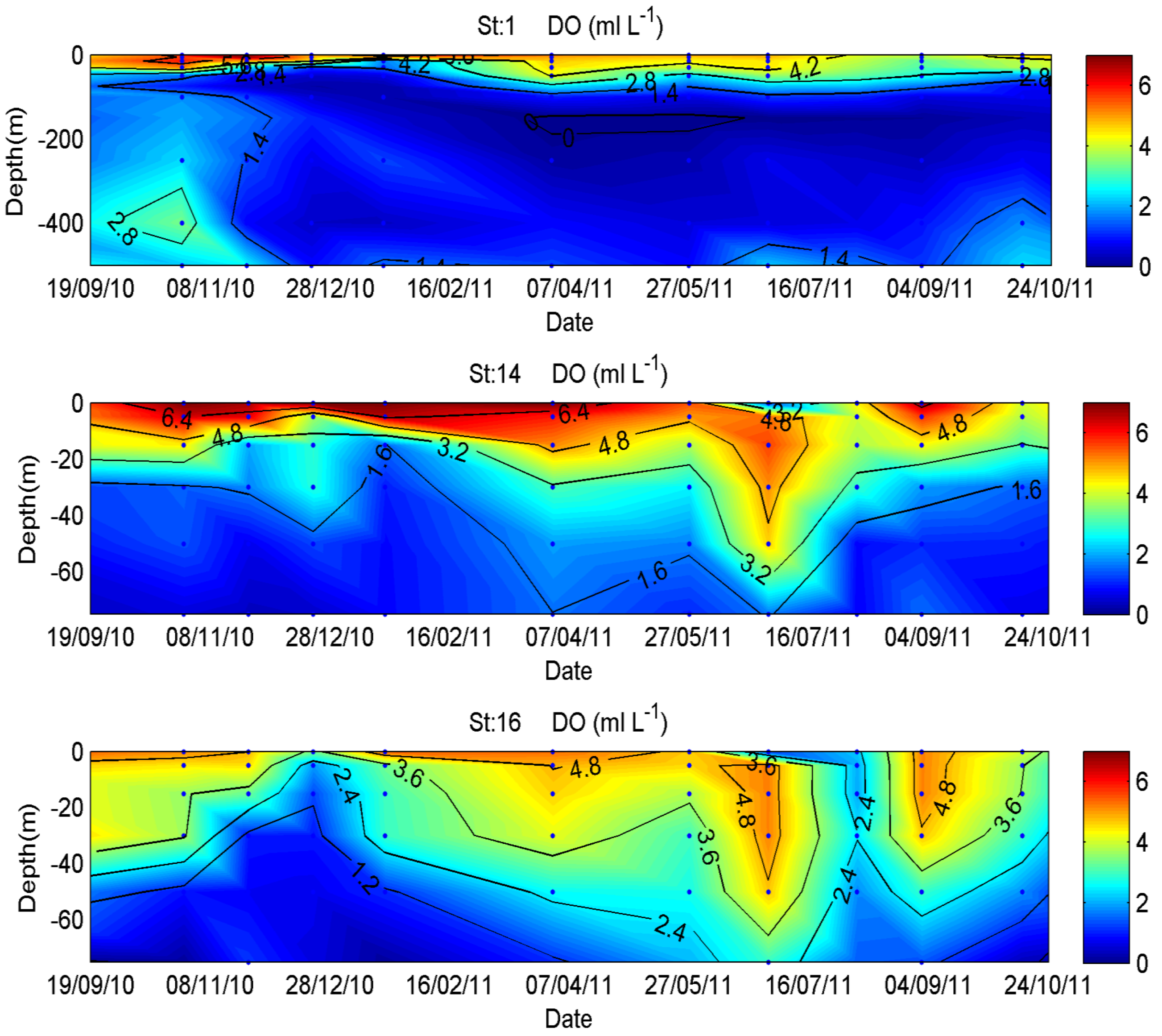

Figure 2. Dissolved Oxygen (DO) time series in the water column measured between October 2010 and January 2011, at stations St1, St14 and St16 off Tongoy Bay, Coquimbo (30°S).

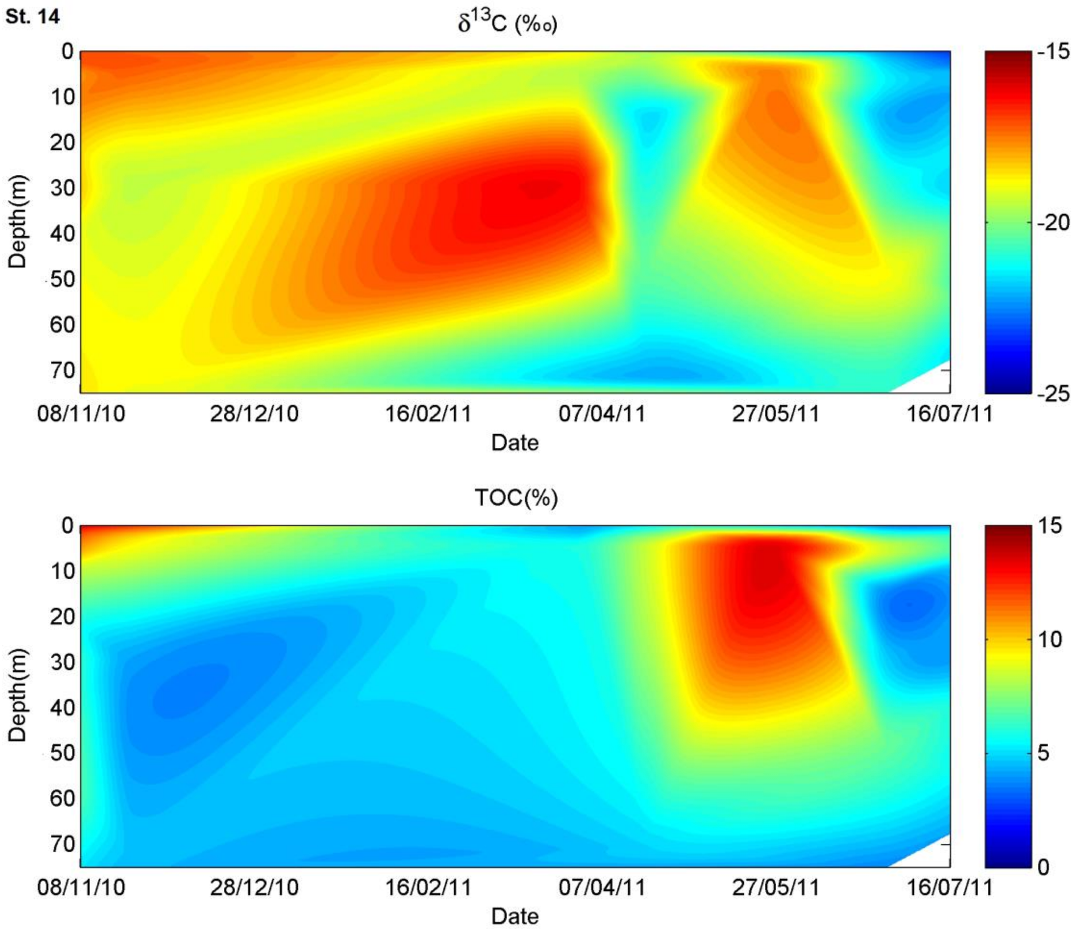

Figure 3. Suspended particulate matter composition (TOC % and δ^{13}Corg) measured in the water column between October 2010 and October 2011, at station St14, Tongoy Bay, Coquimbo (30°S).

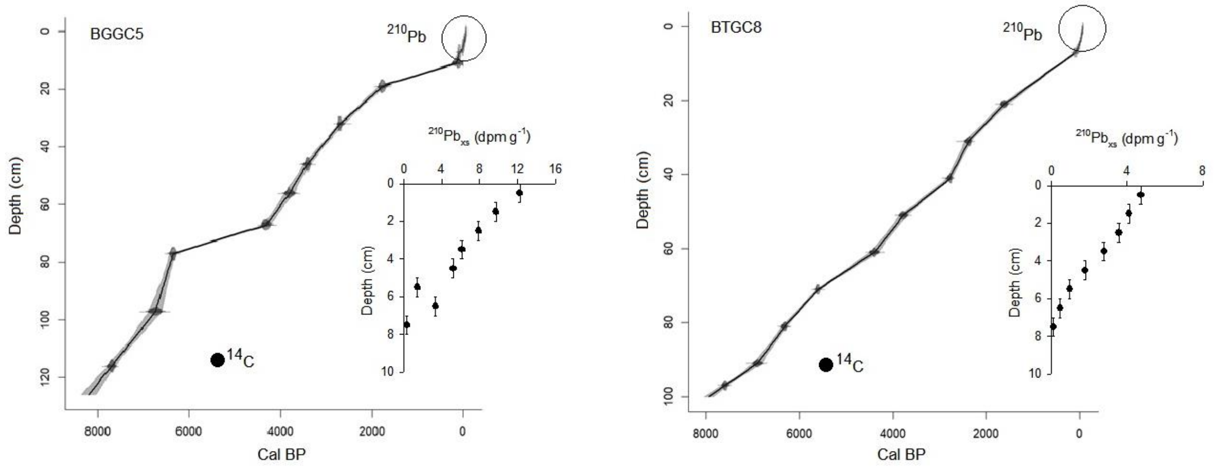

Figure 4. Age model based on ^{14}CAMS and ^{210}Pb measurements. The time scale was obtained according to the best fit of curves of $^{210}Pb_{xs}$ and ^{14}C points using CLAM 2.2 software and Marine curve ^{13}C (Reimer et al., 2013).

a) BGGC5

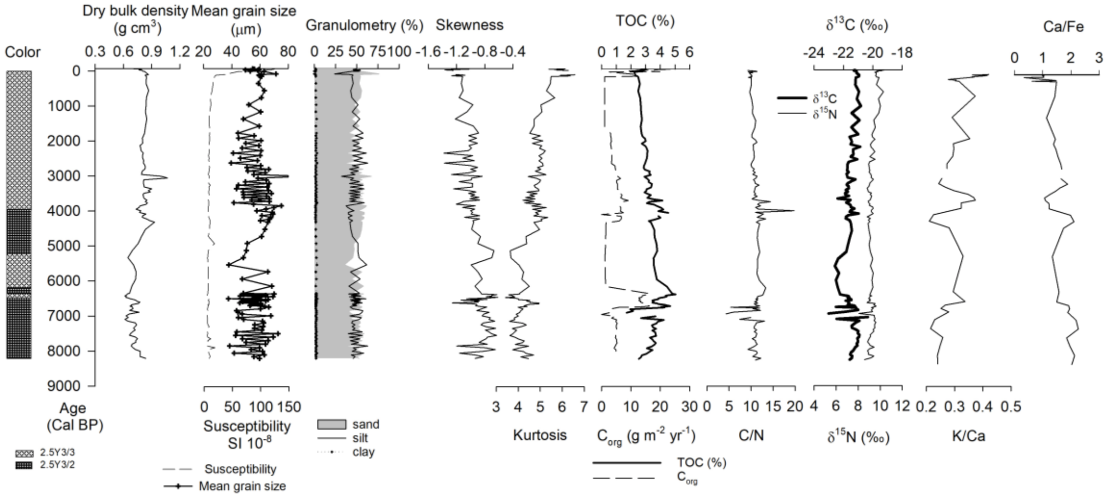

b) BTGC8

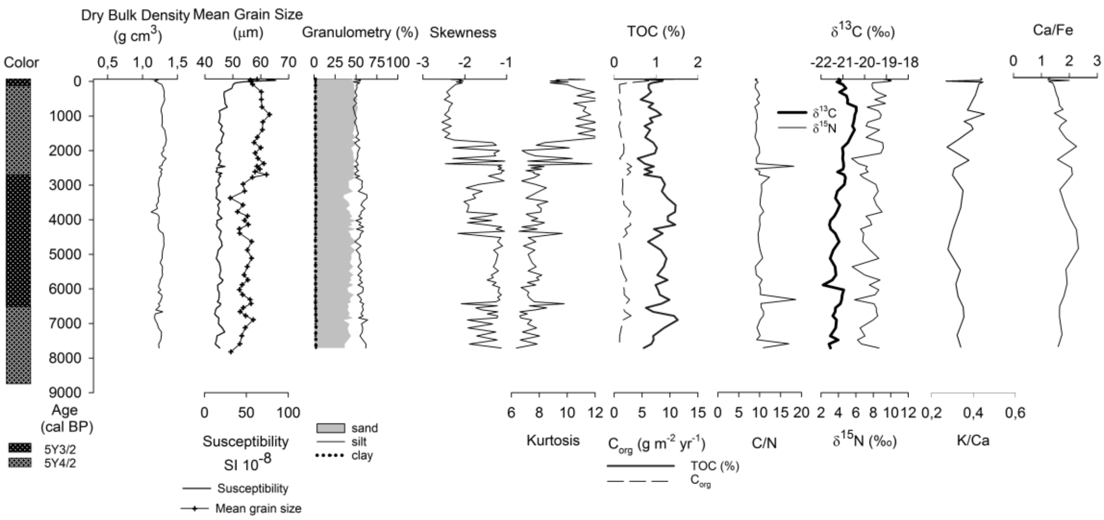

Figure 5. Characterization of sediment cores retrieved from (a) Guanaqueros Bay (BGGC5) and (b) Tongoy Bay (BTGC8). Where is shown the huge (Munsell chart scale) in depth, dry bulk density, mean grain size, granulometry (% sand, silt and clay), statistical parameters (skewness, kurtosis), organic components (TOC, C/N ratio, stable isotopes δ^{15}N and δ^{13}C) and chemical composition (K/Ca, Ca/Fe).

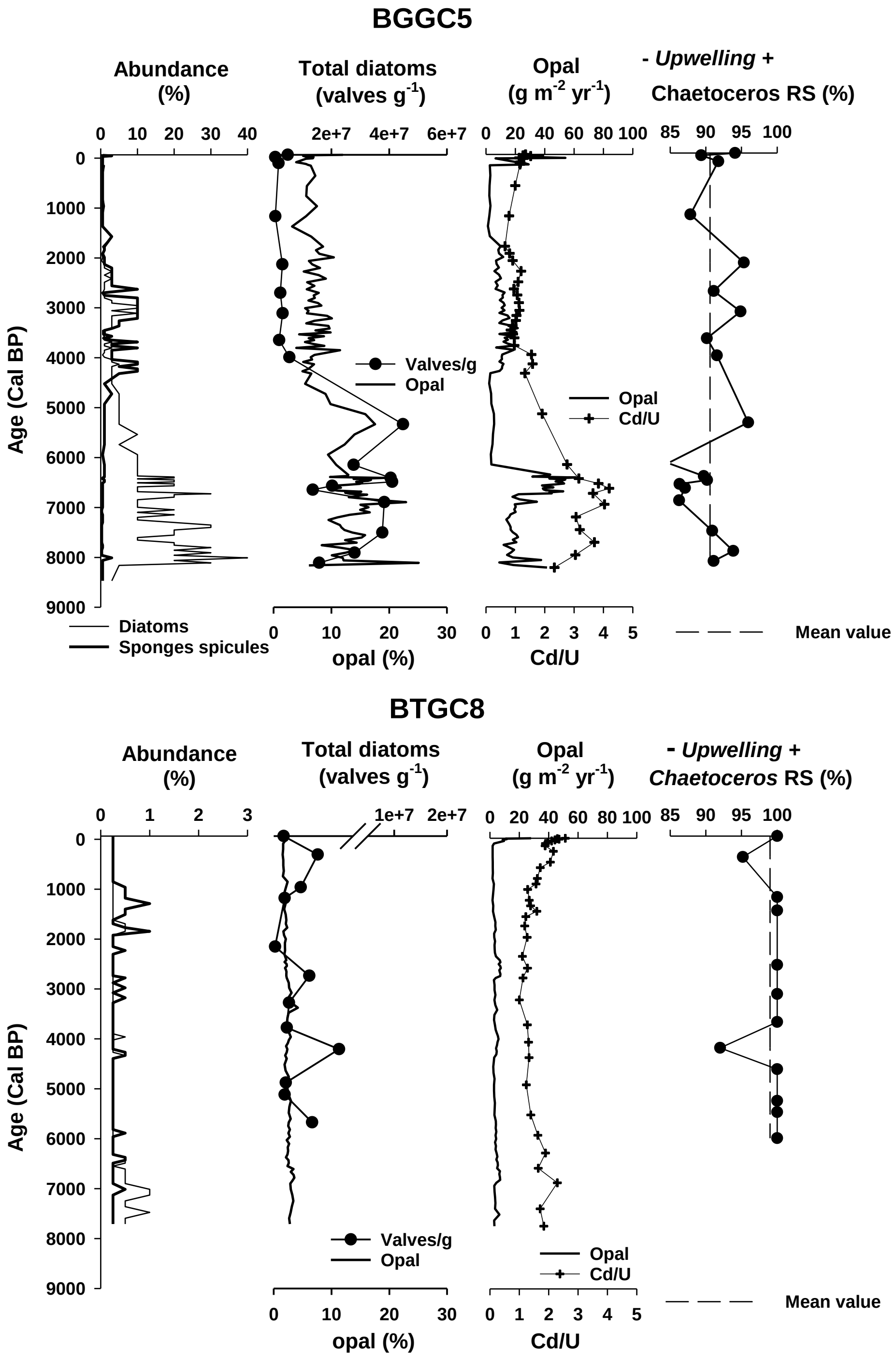

Figure 6. Diatom and sponge spicules relative abundances, total diatom counts (valves g^{-1}) and opal (%), opal accumulation ($g\ m^{-2}\ yr^{-1}$) and Cd/U ratio, and downcore variations in *Ch.* resting spores percentages as proxy of upwelling intensity in BGGC5 and BTGC8 cores (Guanaqueros and Tongoy Bay, respectively), the medium dash line represent the average of *Ch. resting* spore for the respective core. Whereas Cd/U distribution was included as a proxy for redox condition.

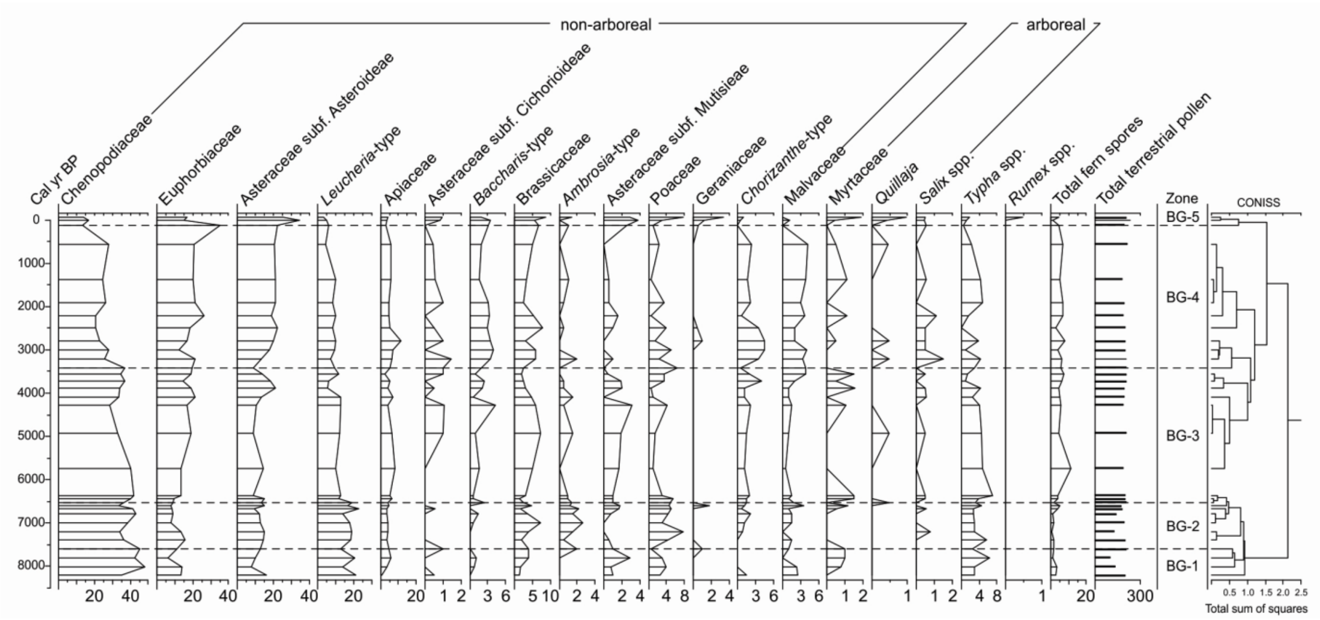

Figure 7. Pollen record in BGGC5 core.

a) BGGC5

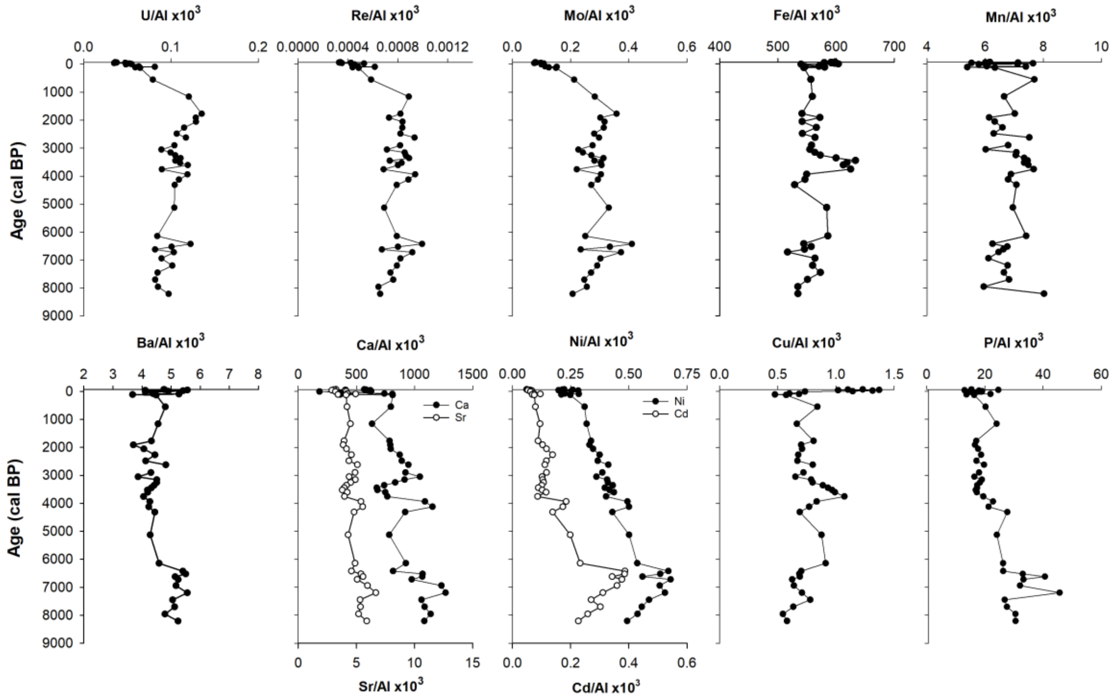

b) BTGC8

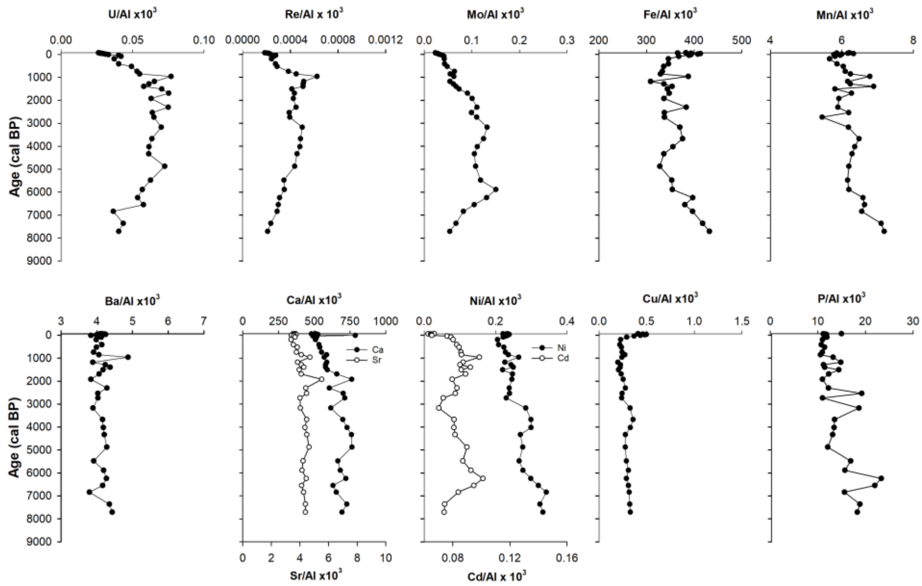

Figure 8. Downcore trace element variations on: (a) Guanaqueros Bay (BGGC5) and (b) Tongoy Bay (BTGC8), off Coquimbo (30°S).

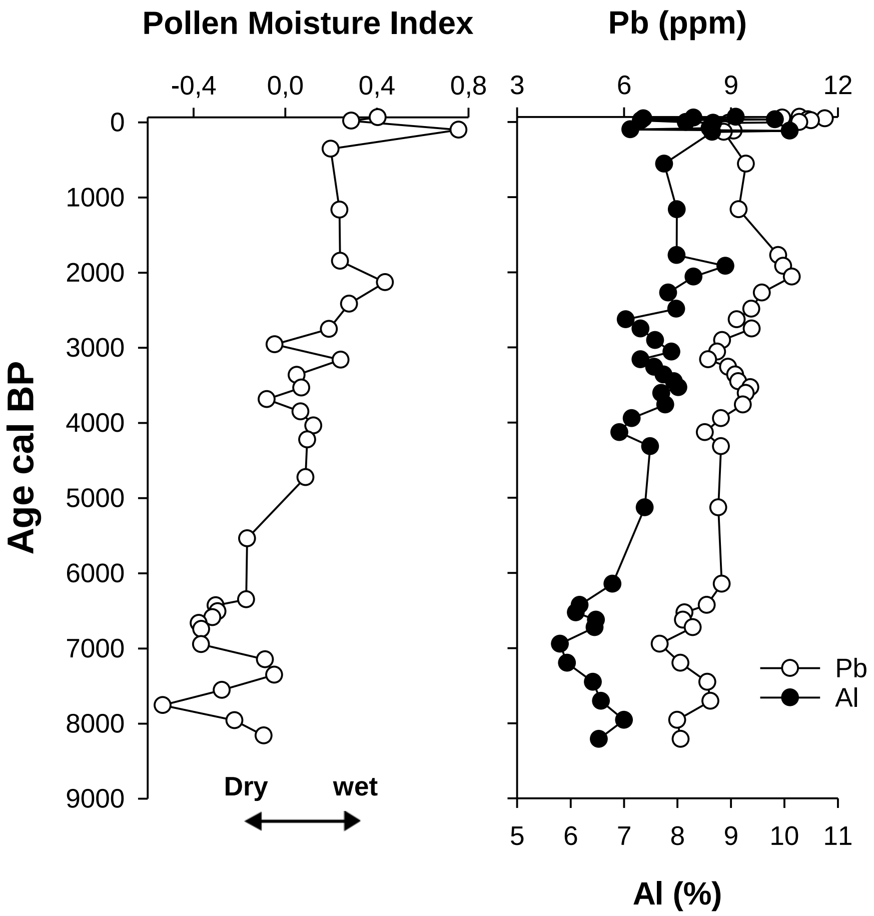

Figure 9. Pollen Moisture Index defined as the normalized ratio between Euphorbiaceae (wet coastal shrub land) and Chenopodiaceae (arid scrubland). Positive (negative) values for this index indicate the relative expansion (reduction) of coastal vegetation under wetter (drier) conditions. Pb and Al distribution at BGGC5 core, representatives of terrigenous input to the bay.